Inorg. Chem. **2003**, *42*, 6204–6224

Symmetry and Geometry Considerations of Atom Transfer: Deoxygenation of $(silox)_3WNO$ and R_3PO (R = Me, Ph, ^tBu) by $(silox)_3M$ (M = V, NbL (L = PMe_3, 4-Picoline), Ta; silox = $^tBu_3SiO$)

Adam S. Veige,[†] LeGrande M. Slaughter,[†] Emil B. Lobkovsky,[†] Peter T. Wolczanski,*[,†] Nikita Matsunaga,[‡] Stephen A. Decker,[§] and Thomas R. Cundari*[,§]

Department of Chemistry & Chemical Biology, Cornell University, Baker Laboratory, Ithaca, New York 14853, Department of Chemistry, Long Island University, Brooklyn, New York 11201, and Department of Chemistry, University of North Texas, Box 305070, Denton, Texas 76203

Received January 13, 2003

Deoxygenations of $(silox)_3WNO$ (**12**) and R_3PO (R = Me, Ph, ^tBu) by $M(silox)_3$ (**1**-M; M = V, NbL (L = PMe_3, 4-picoline), Ta; silox = $^tBu_3SiO$) reflect the consequences of electronic effects enforced by a limiting steric environment. **1**-Ta rapidly deoxygenated R_3PO (23 °C; R = Me ($\Delta G°_{rxn}$(calcd) = –47 kcal/mol), Ph) but not $^tBu_3PO$ (85°, >2 days), and cyclometalation competed with deoxygenation of **12** to $(silox)_3WN$ (**11**) and $(silox)_3TaO$ (**3**-Ta; $\Delta G°_{rxn}$(calcd) = –100 kcal/mol). **1**-V deoxygenated **12** slowly and formed stable adducts $(silox)_3V$-OPR_3 (**3**-OPR_3) with OPR_3. **1**-Nb(4-picoline) (S = 0) and **1**-$NbPMe_3$ (S = 1) deoxygenated R_3PO (23 °C; R = Me ($\Delta G°_{rxn}$(calcd from **1**-Nb) = –47 kcal/mol), Ph) rapidly and **12** slowly ($\Delta G°_{rxn}$(calcd) = –100 kcal/mol), and failed to deoxygenate $^tBu_3PO$. Access to a triplet state is critical for substrate (EO) binding, and the $S \rightarrow T$ barrier of ∼17 kcal/mol (calcd) hinders deoxygenations by **1**-Ta, while **1**-V (S = 1) and **1**-Nb ($S \rightarrow T$ barrier ∼ 2 kcal/mol) are competent. Once binding occurs, significant mixing with an $^1A_1$ excited state derived from population of a σ*-orbital is needed to ensure a low-energy intersystem crossing of the $^3A_2$ (reactant) and $^1A_1$ (product) states. Correlation of a reactant σ*-orbital with a product σ-orbital is required, and the greater the degree of bending in the $(silox)_3M$–O–E angle, the more mixing energetically lowers the intersystem crossing point. The inability of substrates EO = **12** and $^tBu_3PO$ to attain a bent ∠M–O–E due to sterics explains their slow or negligible deoxygenations. Syntheses of relevant compounds and ramifications of the results are discussed. X-ray structural details are provided for **3**-$OPMe_3$ (∠V–O–P = 157.61(9)°), **3**-OP^tBu_3 (∠V–O–P = 180°), **1**-$NbPMe_3$, and $(silox)_3ClWO$ (**9**).

Introduction

Atom transfer is a deceptively simple reaction that is central to various transformations in inorganic chemistry involving formal redox changes among reactants. Oxygen-atom transfers are prominent examples of these inner sphere processes due to their importance and scope.[1] Several biological oxidations involve O-atom transfer from terminal oxo groups, as in cytochrome P450,[2,3] various oxotransferase enzymes, and mimics,[1,4–9] from peroxides in haloperoxidases,[10] or from bridging oxo units, as exemplified by

* Authors to whom correspondence should be addressed. E-mail: ptw2@cornell.edu (P.T.W.); tomc@unt.edu (T.R.C.).
[†] Cornell University.
[‡] Long Island University.
[§] University of North Texas.

(1) (a) Shilov, A. E.; Shteinman, A. A. *Acc. Chem. Res.* **1999**, *32*, 763–771. (b) Woo, L. K. *Chem. Rev.* **1993**, *93*, 1125–1136. (c) Jorgensen, K. A. *Chem. Rev.* **1989**, *89*, 431–458. (d) Holm, R. H. *Coord. Chem. Rev.* **1990**, *100*, 183–221. (e) Holm, R. H. *Chem. Rev.* **1987**, *87*, 1401–1449.

(2) (a) *Cytochrome P450, Structure, Mechanism and Biochemistry*, 2nd ed.; Ortiz de Montellano, P. R., Ed.; Plenum: New York, 1995. (b) Enemark, J. H.; Young, C. G. *Adv. Inorg. Chem.* **1993**, *40*, 1–88.

(3) (a) De Visser, S. P.; Ogliaro, F.; Sharma, P. K.; Shaik, S. *J. Am. Chem. Soc.* **2002**, *124*, 11809–11826. (b) Schoneboom, J. C.; Lin, H.; Reuter, N.; Thiel, W.; Cohen, S.; Ogliaro, F.; Shaik, S. *J. Am. Chem. Soc.* **2002**, *124*, 8142–8151. (c) de Visser, S. P.; Ogliaro, F.; Sharma, P. K. Shaik, S. *Angew. Chem., Int. Ed.* **2002**, *41*, 1947–1950. (d) de Visser, S. P.; Ogliaro, F.; Harris, N.; Shaik, S. *J. Am. Chem. Soc.* **2001**, *123*, 3037–3047. (e) Ogliaro, F.; Harris, N.; Cohen, S.; Filatov, M.; de Visser, S. P.; Shaik, S. *J. Am. Chem. Soc.* **2000**, *122*, 8977–8989.

(4) (a) Hille, R. *Chem. Rev.* **1996**, *96*, 2757–2816. (b) McMaster, J.; Enemark, J. H. *Curr. Opin. Chem. Biol.* **1998**, *2*, 201–207. (c) Romao, M. J.; Huber, R. *Struct. Bonding* **1998**, *90*, 69–95.

10.1021/ic0300114 CCC: $25.00
Published on Web 08/29/2003

methane monoxygenase.[11−14] In the synthesis of fine organics, the utilization of catalytic systems that transfer one[15−17] or two[18−22] oxygens is of increasing importance as regio- and enantioselectivities rise. For inorganic applications, the placement or removal of an oxo group is often a critical synthetic procedure, especially in applications to early transition metal complex synthesis.[23−26] Commodity chemicals synthesis also revolves around oxidation processes that utilize O-atom transfer, including many where dioxygen is the penultimate source.[27]

The transfer of an oxygen atom from a metal−oxo functionality to a substrate, and its microscopic reverse, is a straightforward oxygenation reaction. While the chemistry of $(silox)_3WNO$ (**12**) was being investigated, the identification of $(silox)_3WN$ (**11**) was needed, and deoxygenation of **12** seemed to be a plausible route given Cummins' related preparation of a Cr(VI) nitride from its corresponding Cr(II) nitrosyl.[24] During the course of examining the deoxygenation of a **12** by $(silox)_3M$ (M = Nb (**1**-Nb), Ta (**1**-Ta); silox = $^tBu_3SiO$) some unusual observations were made.[28] Previously, $(silox)_3Ta$ (**1**-Ta) was shown to swiftly strip oxygen atoms from N_2O, NO,[29] CO_2, CO,[30] and epoxides[31] to form $(silox)_3TaO$ (**2**-Ta) below room temperature, yet no O-atom transfer from the tungsten nitrosyl was observed at 23 °C. When an appropriate masked version of its niobium derivative, $(silox)_3Nb(\eta^2$-N,C-4-picoline) (**1**-Nb-4-pic), was examined, the deoxygenation of $(silox)_3WNO$ (**12**) did occur, albeit at elevated temperatures. It was surprising that the tungsten nitrosyl was stable to **1**-Ta under ambient conditions, and was only observed to undergo deoxygenation at significantly higher temperatures with byproduct formation.

Reported herein is a study of the metal dependence on the deoxygenation of $(silox)_3WNO$ (**10**) and R_3PO (R = Me, Ph, ^{t}Bu) by $(silox)_3M$ (M = V, Nb, Ta), replete with synthetic and structural details of the tungsten system and calculational support pertaining to the thermodynamics of the atom transfer events. In this investigation, the symmetry requirements of O-atom transfer and related geometric constraints are revealed. Related interpretations of state selective chemistry have been proferred by Shaik in the actions of cytochrome P450,[3] and Groves in the study of manganese V oxo porphyrin derivatives.[8] While Theopold did not find spin state changes to be consequential in O-atom transfer involving chromium oxo species,[32] Nocera has designed photochemically activated "pac-man" porphyrin systems that take advantage of the preferred side-on geometry for O-atom transfer.[33] It is clear that the tuning of electronic states[34,35]—whether intentional or serendipitous—has profound implications on atom transfer events.

(5) (a) Lim, B. S.; Holm, R. H. *J. Am. Chem. Soc.* **2001**, *123*, 1920−1930. (b) Sung, K. M.; Holm, R. H. *J. Am. Chem. Soc.* **2001**, *123*, 1931−1943.
(6) (a) Pietsch, M. A.; Hall, M. B. *Inorg. Chem.* **1996**, *35*, 1273−1278. (b) Pietsch, M. A.; Couty, M.; Hall, M. B. *J. Phys. Chem.* **1995**, *99*, 16315−16319.
(7) Thomson, L. M.; Hall, M. B. *J. Am. Chem. Soc.* **2001**, *123*, 3995−4002.
(8) (a) Jin, N.; Groves, J. T. *J. Am. Chem. Soc.* **1999**, *121*, 2923−2924. (b) Groves, J. T.; Lee, J.; Marla, S. S. *J. Am. Chem. Soc.* **1997**, *119*, 6269−6273.
(9) Jin, N.; Bourassa, J. L.; Tizio, S. C.; Groves, J. T. *Angew. Chem., Int. Ed.* **2000**, *39*, 3849−3851.
(10) (a) Butler, A. *Coord. Chem. Rev.* **1999**, *187*, 17−35. (b) Butler, A.; Baldwin, A. H. *Struct. Bonding* **1997**, *89*, 109−132.
(11) (a) Merkx, M.; Kopp, D. A.; Sazinsky, M. H.; Blazyk, J. L.; Müller, J.; Lippard, S. J. *Angew. Chem., Int. Ed.* **2001**, *40*, 2782−2807. (b) Wallar, B. J.; Lipscomb, J. D. *Chem. Rev.* **1996**, *96*, 2625−2657. (c) Que, L.; Tolman, W. B. *Angew. Chem., Int. Ed.* **2002**, *41*, 1114−1137.
(12) Ambundo, E. A.; Friesner, R. A.; Lippard, S. J. *J. Am. Chem. Soc.* **2002**, *124*, 8770−8771.
(13) Brazeau, B. J.; Austin, R. N.; Tarr, C.; Groves, J. T.; Lipscomb, J. D. *J. Am. Chem. Soc.* **2001**, *123*, 11831−11837.
(14) Costas, M.; Rohde, J. U.; Stubna, A.; Ho, R. Y. N.; Quaroni, L.; Munck, E.; Que, L. *J. Am. Chem. Soc.* **2001**, *123*, 12931−12932.
(15) (a) Palucki, M.; Finney, N. S.; Pospisil, P. J.; Güler, M. L.; Ishida, T.; Jacobsen, E. N. *J. Am. Chem. Soc.* **1998**, *120*, 948−954. (b) Finney, N. S.; Pospisil, P. J.; Chang, S.; Palucki, M.; Konsler, R. G.; Hansen, K. B.; Jacobsen, E. N. *Angew. Chem., Int. Ed. Engl.* **1997**, *36*, 1720−1723.
(16) Katsuki, T. *Coord. Chem. Rev.* **1995**, *140*, 189−214.
(17) (a) Cavallo, L.; Jacobsen, H. *Chem. Eur. J.* **2001**, *7*, 800−807. (b) Cavallo, L.; Jacobsen, H. *Angew. Chem., Int. Ed.* **2000**, *39*, 589−592. (c) Linde, C.; Åkermark, B.; Norrby, P.-O.; Svensson, M. *J. Am. Chem. Soc.* **1999**, *121*, 5083−5084. (d) Linde, C.; Arnold, M.; Norrby, P.-O.; Åkermark, B. *Angew. Chem., Int. Ed. Engl.* **1997**, *36*, 1723−1725.
(18) (a) Kolb, H. C.; VanNieuwenzhe, M. S.; Sharpless, K. B. *Chem. Rev.* **1994**, *94*, 2483−2547. (b) Andersson, M. A.; Epple, R.; Fokin, V. V.; Sharpless, K. B. *Angew. Chem., Int. Ed.* **2002**, *41*, 472−475.
(19) (a) DelMonte, A. J.; Haller, J.; Houk, K. N.; Sharpless, K. B.; Singleton, D. A.; Strassner, T.; Thomas, A. A. *J. Am. Chem. Soc.* **1997**, *119*, 9907−9908. (b) Norrby, P.-O.; Rasmussen, T.; Haller, J.; Strassner, T.; Houk, K. N. *J. Am. Chem. Soc.* **1999**, *121*, 10186−10192.
(20) Corey, E. J.; Noe, M. C. *J. Am. Chem. Soc.* **1996**, *118*, 11038−11053.
(21) (a) Chen, K.; Costas, M.; Kim, J. H.; Tipton, A. K.; Que, L. *J. Am. Chem. Soc.* **2002**, *124*, 3026−3035. (b) Chen, K.; Costas, M.; Que, L. *J. Chem. Soc., Dalton Trans.* **2002**, 672−679. (c) Costas, M.; Que, L. *Angew. Chem., Int. Ed.* **2002**, *41*, 2179−2181. (d) Ryu, J. K.; Kim, J.; Costas, M.; Chen, K.; Nam, W.; Que, L. *Chem. Commun.* **2002**, 1288−1289.
(22) White, M. C.; Doyle, A. G.; Jacobsen, E. N. *J. Am. Chem. Soc.* **2001**, *123*, 7194−7195.
(23) (a) Ruiz, J.; Vivanco, M.; Floriani, C.; Chiesi-Villa, A.; Guastini, C. *J. Chem. Soc., Chem. Commun.* **1991**, 762−764. (b) Vivanco, M.; Ruiz, J.; Floriani, C.; Chiesi-Villa, A.; Rizzoli, C. *Organometallics* **1993**, *12*, 1802−1810.
(24) Odom, A. L.; Cummins, C. C.; Protasiewicz, J. D. *J. Am. Chem. Soc.* **1995**, *117*, 6613−6614.
(25) (a) Crevier, T. J.; Mayer, J. M. *J. Am. Chem. Soc.* **1997**, *119*, 8485−8491. (b) Hall, K. A.; Mayer, J. M. *J. Am. Chem. Soc.* **1992**, *114*, 10402−10411.
(26) Sung, K.-M.; Holm, R. H. *Inorg. Chem.* **2001**, *40*, 4518−4525.
(27) (a) Parshall, G. W.; Ittel, S. D. *Homogeneous Catalysis*; Wiley-Interscience: New York, 1992. (b) Sheldon, R. A.; Kochi, J. K. *Metal Catalyzed Oxidations of Organic Compounds*; Academic Press: New York, 1981.
(28) Veige, A. S.; Slaughter, L. M.; Wolczanski, P. T.; Matsunaga, N.; Decker, S. A.; Cundari, T. R. *J. Am. Chem. Soc.* **2001**, *123*, 6419−6420.
(29) Veige, A. S.; Kleckley, T. S.; Chamberlin, R. L. M.; Neithamer, D. R.; Lee, C. E.; Wolczanski, P. T.; Lobkovsky, E. B.; Glassey, W. V. *J. Organomet. Chem.* **1999**, *591*, 194−203.
(30) Neithamer, D. R.; LaPointe, R. E.; Wheeler, R. A.; Richeson, D. S.; Van Duyne, G. D.; Wolczanski, P. T. *J. Am. Chem. Soc.* **1989**, *111*, 9056−9072.
(31) Bonanno, J. B.; Henry, T. P.; Neithamer, D. R.; Wolczanski, P. T.; Lobkovsky, E. B. *J. Am. Chem. Soc.* **1996**, *118*, 5132−5133.
(32) Hess, J. S.; Leelasubcharoen, S.; Rheingold, A. L.; Doren, D. J.; Theopold, K. H. *J. Chem. Soc.* **2002**, *124*, 2454−2455.
(33) Pistorio, B. J.; Chang, C. J.; Nocera, D. G. *J. Chem. Soc.* **2002**, *124*, 7884−7885.
(34) (a) Poli, R. *Chem. Rev.* **1996**, *96*, 2135−2204. (b) Poli, R. *Acc. Chem. Res.* **1997**, *30*, 494−501.
(35) Poli, R.; Harvey, J. N. *Chem. Soc. Rev.* **2003**, *32*, 1−8.

Table 1. Selected Characterizations of (silox)$_3$M Derivatives: ^{1}H and ^{13}C{^{1}H} NMR Spectral Data (C_6D_6 unless Otherwise Noted); μ_{eff} in μ_B from Evans Measurements; Elemental Analyses (EA)

compound	^{1}H NMR (δ, assgmt)[a]		^{13}C NMR (δ, assgmt)[b]			μ_{eff} (μ_B)	EA (C,H,N) % calcd (% found)
	((H$_3$C)$_3$C)$_3$	R	*C*(CH$_3$)$_3$	C(*C*H$_3$)$_3$	R		
(^{t}Bu$_3$SiO)$_3$V (**1**-V)	1.95 $\nu_{1/2}$ = 26 Hz		86.25	46.99		2.8	61.98 (60.17) 11.70 (11.89)
(^{t}Bu$_3$SiO)$_3$VO (**2**-V)[c]	1.33		25.08	31.28			60.59 (60.09) 11.44 (10.89)
(^{t}Bu$_3$SiO)$_3$VOPMe$_3$ (**3**-OPMe$_3$)	1.77 $\nu_{1/2}$ = 352 Hz	*d*	156.18	39.90	*d*	2.8	59.32 (57.26) 11.49 (11.60)
(^{t}Bu$_3$SiO)$_3$VOPPh$_3$ (**3**-OPPh$_3$)	1.75 $\nu_{1/2}$ = 440 Hz	*e*	145.45	39.95	*e*	2.7	66.46 (66.25) 9.92 (9.69)
(^{t}Bu$_3$SiO)$_3$VOP^{t}Bu$_3$ (**3**-OP^{t}Bu$_3$)	1.82 $\nu_{1/2}$ = 456 Hz	*f*	*f*			2.6	62.94 (59.26) 11.88 (11.33)
(^{t}Bu$_3$SiO)$_3$NbPMe$_3$[g,h] (**1**-NbPMe$_3$)	1.69 $\nu_{1/2}$ = 33 Hz	34.60 (PMe) $\nu_{1/2}$ = 336 Hz	229.75	83.15	*d*	2.4	57.44 (56.15) 11.13 (11.10)
(^{t}Bu$_3$SiO)$_3$ClWO (**7**)	1.35		25.43	30.89			49.05 (49.07) 9.26 (8.99)
(^{t}Bu$_3$SiO)$_3$WO (**8**)	2.32 $\nu_{1/2}$ = 15 Hz		88.52	72.68		1.2	51.10 (49.18) 9.65 (9.36)
(^{t}Bu$_3$SiO)$_3$ClWNO (**9**)	0.97 $\nu_{1/2}$ = 9 Hz		121.00	22.65			
(^{t}Bu$_3$SiO)$_3$WNO (**10**)	1.25		23.65	30.80			50.27 (49.98) 9.49 (9.56) 1.63 (1.58)
(^{t}Bu$_3$SiO)$_3$WN (**11**)	1.30		24.61	30.98			51.22 (51.19) 10.36 (9.49) 1.66 (1.52)
(^{t}Bu$_3$SiO)$_2$HTaOSi^{t}Bu$_2$-CMe$_2$CH$_2$ (**12**-Ta)[i]	1.27	21.97 (H)	23.61	30.73	23.52 (SiC)		*i*
		1.29 (^{t}Bu)			24.93 (SiCMe$_2$)		
		1.37 (Me$_2$)			33.61 (C(*C*H$_3$)$_3$)$_2$		
		1.89 (br, CH$_2$)			39.80 (C(*C*H$_3$)$_2$)		
					97.04 (CH$_2$)		
(^{t}Bu$_3$SiO)$_2$HNbOSi^{t}Bu$_2$-CMe$_2$CH$_2$ (**12**-Nb)[j,k]	1.25	11.66, 12.44 (H)	23.72	30.49	23.50, 23.57 (SiC)		
		1.25 (^{t}Bu)			30.71 (SiCMe$_2$)		
		1.37 (Me$_2$)			31.95, 32.01 (C(*C*H$_3$)$_3$)$_2$		
		2.25, 2.78 (CH$_2$)			39.51, 39.77 (C(*C*H$_3$)$_2$)		
					85.24, 94.16 (CH$_2$)		

[a] Referenced to C_6D_5H at δ 7.15. [b] Referenced to C_6D_6 at δ 128.00. [c] With Cl_3VO serving as an external reference, its ^{51}V NMR resonance is at δ −733.7. [d] PMe_3 not observed. [e] PPh_3 not observed/assigned. [f] P^{t}Bu$_3$ not observed/assigned, and poor solubility hampered data aquisition. [g] Referenced to C_7D_7H (toluene) methyl proton at δ 2.09. [h] Referenced to C_7D_8 (toluene) methyl carbon at δ 24.04. [i] See ref 55. [j] Assignments based on correlation with **12**-Ta. [k] Two isomers are evident (isomer A:isomer B in ^{1}H NMR spectrum ∼ 1.8:1).

Results

Synthesis and Characterization. 1. (silox)$_3$V (1-V). Treatment of {(Me$_3$Si)$_2$N}$_3$V[36] with (silox)H in hexanes for 1.5 h afforded purple (silox)$_3$V (**1**-V) in 74% yield upon crystallization from pentane (eq 1). **1**-V exhibits a broad

$$\{(Me_3Si)_2N\}_3V + 3(silox)H \xrightarrow[\text{hexanes}]{23\ ^\circ C,\ 1.5\ h} \underset{\mathbf{1}\text{-V}}{(silox)_3V} + 3(Me_3Si)_2NH \quad (1)$$

signal ($\nu_{1/2}$ = 26 Hz) in its ^{1}H NMR spectrum at δ 1.95 and broadened ^{13}C NMR spectroscopic resonances at δ 86.25 (Me) and 46.99 (SiC) characteristic of the silox group (Table 1.). An Evans measurement[37] revealed μ_{eff} to be 2.8 μ_B, which is typical for an S = 1, d^2, 3-coordinate vanadium center.[38]

2. (silox)$_3$VO (2-V). (silox)$_3$V (**1**-V) was exposed to excess N_2O in benzene solution until the color became off-white,[39] indicating the formation of (silox)$_3$VO (**2**-V), which could be isolated in 72% yield as a powder upon removal of solvent. **2**-V is a diamagnetic compound, and possesses NMR

$$(silox)_3V + N_2O\ (\text{excess}) \xrightarrow[\text{benzene}]{23\ ^\circ C,\ 45\ \text{min}} \underset{\mathbf{2}\text{-V}}{(silox)_3VO} + N_2 \quad (2)$$

spectral characteristics (Table 1) similar to those of (silox)$_3$MO (M = Nb, **2**-Nb;[29] Ta, **2**-Ta).[30] Infrared spectral evidence for the oxo ligand was not obtained due to overlap with ligand absorptions.

3. (silox)$_3$VOPR$_3$ (3-OPR$_3$, R = Me, Ph, ^{t}Bu). Treatment of (silox)$_3$V (**1**-V) with R$_3$PO (R = Me, Ph, ^{t}Bu) provided the crystalline, green adducts (silox)$_3$V-OPR$_3$ (**3**-OPR$_3$; R = Me (60%), Ph (80%), ^{t}Bu (75%)). Evans measurements[37] revealed μ_{eff} to be 2.7(1) μ_B for each complex, consistent

$$(silox)_3V + R_3PO \xrightarrow[\text{benzene}]{23\ ^\circ C} \underset{\mathbf{3}\text{-OPR}_3\ (R = Me, Ph, {}^t\text{Bu})}{(silox)_3V\text{-OPR}_3} \quad (3)$$

with an S = 1, d^2, pseudotetrahedral vanadium.[38] ^{1}H and

(36) Alyea, E. C.; Bradley, D. C.; Copperthwaite, R. G. *J. Chem. Soc., Dalton Trans.* **1972**, 1580−1584.
(37) (a) Evans, D. F. *J. Chem. Soc.* **1959**, 2003−2005. (b) Orrell, K. G.; Sik, V. *Anal. Chem.* **1980**, *52*, 567−569. (c) Schubert, E. M. *J. Chem. Educ.* **1992**, *69*, 62.
(38) Drago, R. S. *Physical Methods for Chemists*; Saunders: New York, 1992.
(39) Neithamer, D. R. Ph.D. Thesis, Cornell University, 1989.

Table 2. Crystallographic Data for $(silox)_3V\text{-}OPR_3$ (**3**-OPR_3; R = Me, ^{t}Bu), $(silox)_3NbPMe_3$ (**1**-$NbPMe_3$), and $(silox)_3ClWO$ (**7**)

	3-$OPMe_3$	**3**-OP^tBu_3[a]	**1**-$NbPMe_3$	**7**
formula	$C_{39}H_{90}VO_4PSi_3$	$C_{48}H_{108}VO_4PSi_3$	$C_{39}H_{90}NbO_3PSi_3$	$C_{36}H_{81}ClO_4Si_3W$
fw	789.29	915.52	815.26	881.58
space group	$P2_1/n$	$P31c$	$C2/c$	$P2_1$
Z	4	2	8	2
a, Å	13.2336(12)	16.587(7)	46.322(7)	8.7021(1)
b, Å	17.4681(17)	16.587(7)	12.8527(14)	21.0660(3)
c, Å	21.070(2)	12.883(7)	18.580(3)	12.5399(2)
α, deg	90	90	90	90
β, deg	90.294 (2)	90	92.718(11)	105.5070(7)
γ, deg	90	120	90	90
V, Å^3	4870.7(8)	3070(2)	11050(3)	2215.11(5)
ρ_{calcd}, g cm^{-3}	1.076	0.991	0.980	1.322
μ, mm^{-1}	0.343	0.279	0.338	2.781
temp, K	193(2)	173(2)	243	173(2)
λ (Å)	0.71073	0.71073	0.71073	0.71073
R indices [$I > 2\sigma(I)$][b,c]	$R_1 = 0.0309$	$R_1 = 0.0735$	$R_1 = 0.0398$	$R_1 = 0.0345$
	$wR_2 = 0.0906$	$wR_2 = 0.1965$	$wR_2 = 0.1153$	$wR_2 = 0.0904$
R indices (all data)[b,c]	$R_1 = 0.0374$	$R_1 = 0.0817$	$R_1 = 0.0550$	$R_1 = 0.0364$
	$wR_2 = 0.0984$	$wR_2 = 0.2043$	$wR_2 = 0.1302$	$wR_2 = 0.0915$
GOF[d]	1.022	1.074	0.914	1.065

[a] The asymmetric unit is $^1/_3$ of the formula unit. [b] $R_1 = \sum||F_o| - |F_c||/\sum|F_o|$. [c] $wR_2 = [\sum w(|F_o| - |F_c|)^2/\sum\omega F_o^2]^{1/2}$. [d] GOF (all data) = $[\sum w(|F_o| - |F_c|)^2/(n - p)]^{1/2}$, n = number of independent reflections, p = number of parameters.

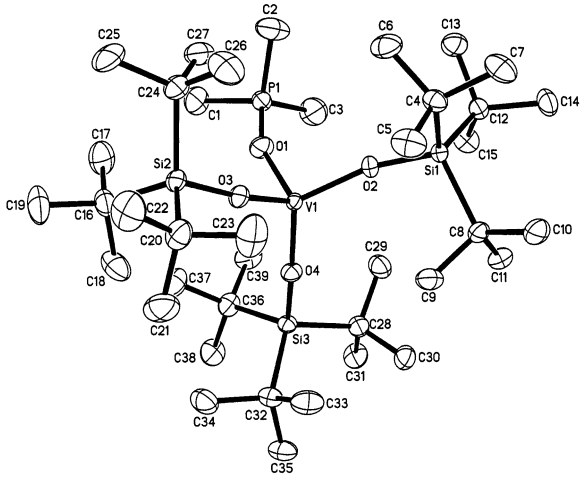

Figure 1. Molecular view (40% ellipsoids) of $(silox)_3VOPMe_3$ (**3**-$OPMe_3$).

$^{13}C\{^1H\}$ NMR spectral characteristics for **3**-$OPMe_3$ and **3**-$OPPh_3$ were consistent with paramagnetic species, as was the silox portion of the ^{1}H NMR spectrum of **3**-OP^tBu_3 (Table 1), whose $^{13}C\{^1H\}$ NMR spectrum was unable to be determined due to solubility difficulties. ^{1}H NMR spectral signals for the PR_3 fragments either were not observed or could not be assigned with confidence.

4. Structure of $(silox)_3VOPMe_3$ (3-$OPMe_3$). An X-ray structure determination (Table 2) of $(silox)_3VOPMe_3$ (**3**-$OPMe_3$) revealed near tetrahedral symmetry at the core, as Figure 1 illustrates. The silox d(V−O) of 1.8593(12), 1.8541(12), and 1.8519(12) Å[40] are noticeably different from the phosphine oxide−vanadium distance of 1.9906(13) Å. The P−O−V linkage of the datively bonded ligand is clearly bent (157.61(9)°), and the comparative silox angle (∠Si−O−V = 160.34(9)°, 164.48(9)°, 169.93(8)°) is somewhat straighter. Intersilox repulsions render the SiO−V−OSi angles (114.30(6)°, 116.61(6)°, and 116.92(5)°) wider than the SiO−V−OP angles (100.16(6)°, 101.08(6)°, and 104.12(6)°). The ^{t}Bu$_3$Si groups are typical for the silox ligand, and the geometry about the phosphorus is roughly tetrahedral (∠C−P−O_{av} = 112.0(19)°, ∠C−P−C_{av} = 106.9(4)°), and perhaps reflective of the steric influence of the siloxes. Detailed geometric data is given in Table 3.

Table 3. Interatomic Distances (Å) and Angles (deg) Pertaining to $(silox)_3VOPMe_3$ (**3**-$OPMe_3$)

V−O2	1.8593(12)	V−O3	1.8541(12)	V−O4	1.8519(12)
V−O1	1.9906(13)	Si1−O2	1.6344(12)	Si2−O3	1.6325(12)
Si3−O4	1.6287(12)	O1−P	1.4964(14)	P−C1	1.782(2)
P−C2	1.784(2)	P−C3	1.780(2)	Si−C_{av}	1.936(3)
C−C_{av}	1.541(6)				

O1−V−O2	100.16(6)	O1−V−O3	104.12(6)	O1−V−O4	101.08(6)
O2−V−O3	116.61(6)	O2−V−O4	116.92(5)	O3−V−O4	114.30(6)
V−O2−Si1	160.34(9)	V−O3−Si2	164.48(9)	V−O4−Si3	169.93(8)
V−O1−P	157.61(9)	O1−P−C1	109.71(10)	O1−P−C2	113.06(11)
O1−P−C3	113.10(11)	C1−P−C2	107.21(13)	C1−P−C3	106.94(14)
C2−P−C3	106.47(13)	O−Si−C_{av}	107.5(4)	C−Si−C_{av}	111.3(6)
Si−C−C_{av}	111.6(20)	C−C−C_{av}	107.2(11)		

5. Structure of $(silox)_3VOP^tBu_3$ (3-$OP\ ^tBu_3$). An X-ray structure determination of $(silox)_3VOP^tBu_3$ (**3**-OP^tBu_3) in the trigonal crystal system (Table 2) revealed a unique silox group, one P^{t}Bu fragment, and a crystallographically imposed linear V−O−P linkage (Figure 2.). All the ^{t}Bu groups are relatively normal, as the distances in Table 4 reveal, and the d(V−OSi) of 1.882(6) Å[40] contrasts with the longer dative interaction of the phosphine oxide (d(V−OP) = 2.083(9) Å). In comparison to $(silox)_3VOPMe_3$ (**3**-$OPMe_3$), the greater vanadium−oxygen distances reflect the severe steric requirements of the OP^tBu_3 ligand; the phosphine oxide−vanadium interaction is almost 0.1 Å longer. Because of the shorter vanadium−oxygen distances of the silox ligands, steric repulsion among them is greater (∠SiO−V−OSi = 114.18(14)°) than the silox/OP^tBu_3 interactions (∠SiO−V−OP = 104.2(2)°). As usual, the Si−O−V angle approaches linearity

(40) (a) Henderson, R. A.; Janas, Z.; Jerzykiewicz, L. B.; Richards, R. L.; Sobota, P. *Inorg. Chim. Acta* **1999**, *285*, 178−183. (b) Henderson, R. A.; Hughes, D. L.; Janas, Z.; Richards, R. L.; Sobota, P.; Szafert, S. *J. Organomet. Chem.* **1998**, *554*, 195−201. (c) Scott, M. J.; Wilisch, W. C. A.; Armstrong, W. H. *J. Am. Chem. Soc.* **1990**, *112*, 2429−2430. (d) Wilisch, W. C. A.; Scott, M. J.; Armstrong, W. H. *Inorg. Chem.* **1988**, *27*, 4333−4335. (e) Carrano, C. J.; Mohan, M.; Holmes, S. M.; de la Rosa, R.; Butler, A.; Charnock, J. M.; Garner, C. D. *Inorg. Chem.* **1994**, *33*, 646−655.

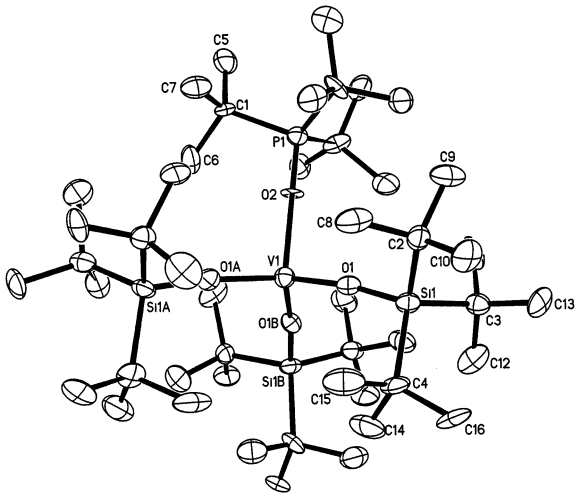

Figure 2. Molecular view (40% ellipsoids) of $(silox)_3VOP^tBu_3$ (**3**-OP^tBu_3).

Table 4. Interatomic Distances (Å) and Angles (deg) Pertaining to $(silox)_3VOP^tBu_3$ (**3**-O P^tBu_3)

V−O1	1.882(6)	O1−Si1	1.642(7)	P−C1	1.867(10)
V−O2	2.083(9)	O2−P	1.466(10)	C1−C_{av}	1.556(36)
Si1−C2	1.933(11)	Si1−C3	1.954(11)	Si1−C4	1.934(11)
C2−C_{av}	1.550(49)	C3−C_{av}	1.504(28)	C4−C_{av}	1.531(41)
SiO−V−OSi	114.18(14)	SiO−V−O2	104.2(2)	C−P−C	110.8(3)
V−O1−Si	171.8(4)	V−O2−P	180	O2−P−C1	108.1(3)
O1−Si1−C2	108.2(5)	O1−Si1−C3	108.3(5)	O1−Si1−C4	109.7(4)
Si1−C2−C_{av}	112.6(25)	Si1−C3−C_{av}	111.2(38)	Si1−C4−C_{av}	111.0(38)
C−Si−C_{av}	110.2(3)	P−C1−C_{av}	110.1(26)	C−C(Si)-C_{av}	107.2(16)
C−C(P)-C_{av}	108.8(6)				

(171.8(4)°), presumably due to the steric constraints around the first-row metal.

6. $(silox)_3NbPMe_3$ (1-$NbPMe_3$). Reduction of $(silox)_3NbCl_2$ (**4**) with Na/Hg in neat PMe_3 afforded purple $(silox)_3NbPMe_3$ (**1**-$NbPMe_3$) in 53% yield upon crystallization from hexanes.

$$\underset{\mathbf{4}}{(silox)_3NbCl_2} \xrightarrow[\text{Na/Hg, } PMe_3]{\text{23 °C, 12 h, } PMe_3} \underset{\mathbf{1}\text{-}NbPMe_3}{(silox)_3NbPMe_3} \qquad (4)$$

A μ_{eff} of 2.4 μ_B was determined via the Evans method,[37] consistent with a pseudotetrahedral d^2 system ($S = 1$), and the observation of the silox ^{t}Bu protons at δ 1.69 ($\nu_{1/2} = 33$ Hz) and the phosphine methyls as a very broad resonance at δ 34.60 ($\nu_{1/2} = 336$ Hz) in the ^{1}H NMR spectrum. In the $^{13}C\{^1H\}$ NMR spectrum, the tertiary carbons are markedly affected by the paramagnetism of **1**-$NbPMe_3$ and are observed at δ 229.75. Even the silox methyls shift dramatically to δ 83.15, and no resonance could be confidently assigned to the PMe_3 ligand; no resonance was observed in the $^{31}P\{^1H\}$ spectrum either. Niobium(III) is typically found in dimeric or cluster derivatives,[41,42] so this simple coordination compound is quite unusual.

7. Structure of $(silox)_3NbPMe_3$ (1-$NbPMe_3$). An X-ray structural determination (Table 2, Table 5) of $(silox)_3NbPMe_3$ (**1**-$NbPMe_3$) revealed a flattened tetrahedral geometry that is nearly pyramidal (Figure 3), with ∠PNbO = 101.1(19)° (av) and ∠ONbO = 116.3(6)° (av). The d(NbO) = 1.948(8) Å (av) and d(NbP) = 2.4923(7) Å are normal (e.g., r_{cov}(Nb) + r_{cov}(P) = 1.34 + 1.06 = 2.40 Å), and the silox ligands display their usual 3-fold splay about the niobium center, with ∠NbOSi = 167.6(13)°.

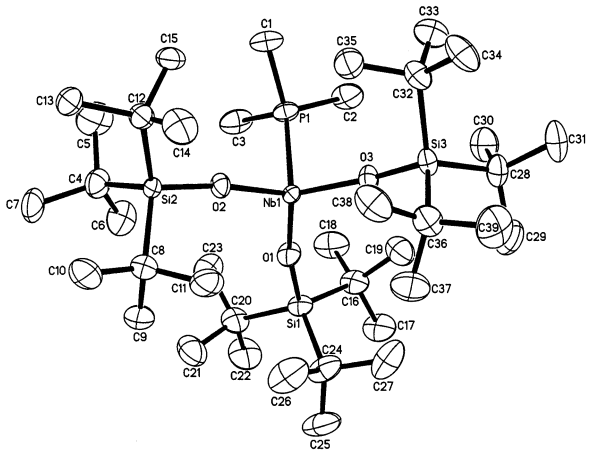

Figure 3. Molecular view (40% ellipsoids) of $(silox)_3NbPMe_3$ (**1**-$NbPMe_3$).

Table 5. Selected Interatomic Distances (Å) and Angles (deg) for $(silox)_3NbPMe_3$ (**1**-$NbPMe_3$)

Nb−P	2.4923(7)	Nb−O1	1.9433(17)	Nb−O2	1.9438(16)
Nb−O3	1.9572(17)	O1−Si1	1.6300(18)	O2−Si2	1.6292(17)
O3−Si3	1.6345(18)	P−C1	1.809(3)	P−C2	1.816(4)
P−C3	1.819(4)	Si−C_{av}	1.925(12)	C−C_{av}	1.540(17)
P−Nb−O1	99.77(7)	O1−Nb−O2	115.91(8)	Nb−O1−Si1	166.70(13)
P−Nb−O2	103.33(6)	O1−Nb−O3	116.97(8)	Nb−O2−Si2	169.05(11)
P−Nb−O3	100.41(6)	O2−Nb−O3	116.16(7)	Nb−O3−Si3	167.07(12)
Nb−P−C1	118.95(11)	Nb−P−C2	116.87(13)	Nb−P−C3	114.01(13)
C1−P−C2	100.96(18)	C1−P−C3	101.29(17)	C2−P−C3	102.2(2)
O−Si−C_{av}	107.3(8)	C−Si−C_{av}	111.5(6)	Si−C−C_{av}	111.4(18)
C−C−C_{av}	107.4(14)				

8. $(silox)_3W$ Derivatives. Treatment of $(silox)_3WCl$ (**6**), prepared from reduction of $(silox)_3WCl_2$ (**5**),[43] with 1 equiv of N_2O afforded the C_{3v} (vide infra) oxo derivative $(silox)_3ClWO$ (**7**, 60%), and N_2 according to Scheme 1. Sharp resonances were observed in the NMR spectra, and a band at 920 cm^{-1} was tentatively assigned to the ν(WO).[44] This is on the low end of the normal range of 920−1058 cm^{-1} for tungsten−oxo complexes,[45,46] perhaps suggesting that the chloride exerts a substantial trans influence. Reduction of **7** with 1.5 equiv of Na/Hg in THF afforded a purple solution that gave gray-green $(silox)_3WO$ (**8**) upon trituration with hexanes and recrystallizations from pentane (22%). The W(V) oxo derivative was characterized by broad resonances in the ^{1}H NMR spectrum at δ 2.32 ($\nu_{1/2} = 15$

(41) Tayebani, M.; Conoci, S.; Feghali, K.; Gambarotta, S.; Yap, G. P. A. *Organometallics* **2000**, *19*, 4568−4574.
(42) (a) Caselli, A.; Solari, E.; Scopelliti, R.; Floriani, C.; Re, N.; Rizzoli, C.; Chiesi-Villa, A. *J. Am. Chem. Soc.* **2000**, *122*, 3652−3670. (b) Kawaguchi, H.; Matsuo, T. *Angew. Chem., Int. Ed.* **2002**, *41*, 2792−2794.
(43) For the X-ray crystal structures (e.g., $(silox)_3WCl_2$ (**5**, tbp, axial Cl's) and $(silox)_3WCl$ (**6**, highly dist sq pl)) and chemistry of silox tungsten chlorides, see: (a) Majol, A.-R. Ph.D. Thesis, Cornell University, 1999. (b) Chamberlin, R. L.; Douthwaite, R. E.; Majol, A.-R.; Slaughter, L. M.; Veige, A. S.; Wolczanski, P. T. Manuscript in preparation.
(44) A DFT calculation on $(HO)_3ClWO$ (**7′**), which modeled $(silox)_3ClWO$ (**7**), revealed a ν(WO) of 945 cm^{-1}; significant coupling with the axial Cl or the oxygens was not noted.
(45) Parkin, G.; Bercaw, J. E. *Polyhedron* **1988**, *7*, 2053−2082.
(46) Nugent, W. A.; Mayer, J. M., *Metal-Ligand Multiple Bonds*; John Wiley & Sons: New York, 1988.

Scheme 1

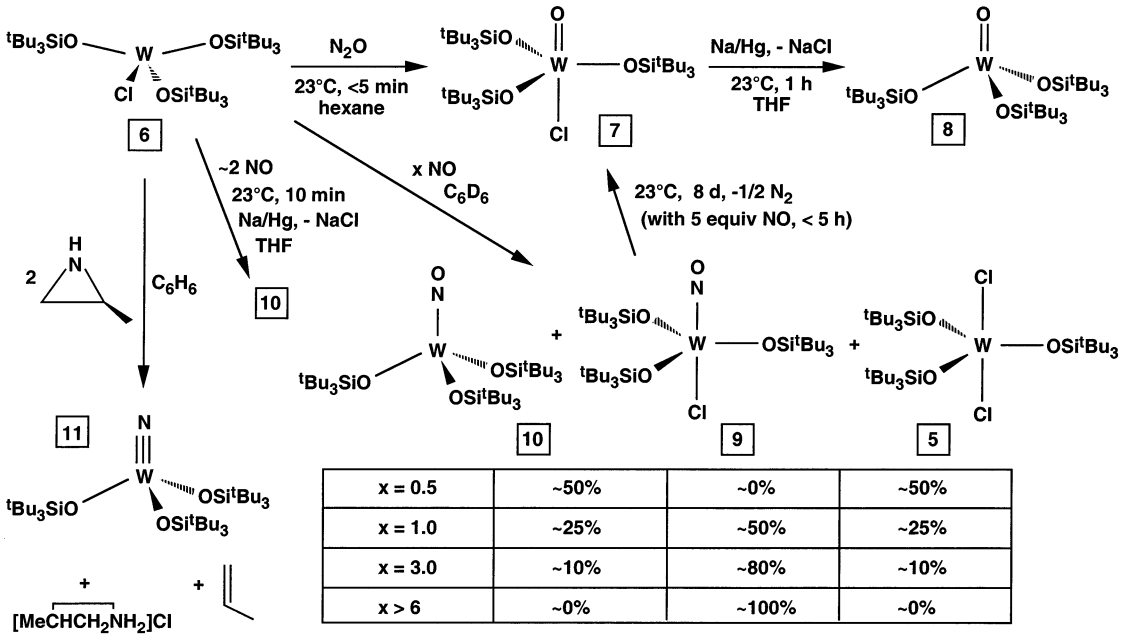

x = 0.5	~50%	~0%	~50%
x = 1.0	~25%	~50%	~25%
x = 3.0	~10%	~80%	~10%
x > 6	~0%	~100%	~0%

Hz) and in the $^{13}C\{^1H\}$ NMR spectrum at δ 72.68 (CH_3) and δ 88.52 (CMe_3), and a μ_{eff} of 1.2 μ_B (Evans method). A ν(WO) of 909 cm^{-1} was observed in its IR spectrum, and this tentative assignment is consistent with the expected lowering of the oxo stretch from that of the W(VI) derivative, **7**, due to occupation of a d-orbital with some π* character.

Exposure of $(silox)_3WCl$ (**6**) to 1 equiv of NO in a sealed NMR tube (C_6D_6) rapidly (<5 min, 23 °C) provided three products in a rough 2:1:1 ratio: nitrosyl chloride $(silox)_3ClWNO$ (**9**), dichloride **5**, and nitrosyl $(silox)_3WNO$ (**10**). Over the course of 8 days (23 °C), it is likely that only the nitrosyl chloride was converted to $(silox)_3ClWO$ (**7**) and $^1/_2N_2$, because the ratio of **7**/**9**:**5**:**10** remained constant. Formation of the dichloride (**5**) and W(II) nitrosyl **10** is a plausible consequence of chlorine-atom transfer between the nitrosyl chloride (**9**) and the starting monochloride (**6**). When **6** was treated with only $^1/_2$ equiv of NO under indentical conditions, the dichloride (**5**) and nitrosyl **10** formed in a 1:1 ratio. Given the likelihood that Cl-atom transfer could disrupt attempts to synthesize pure $(silox)_3ClWNO$ (**9**), $(silox)_3WCl$ (**6**) was exposed to a greater excess (6 equiv) of NO. Unfortunately, this only accelerated the degradation of **9** to oxo chloride **7**, and under a vast excess of NO, this route provided an alternative means to cleanly synthesize **7**.

Because of these complications, $(silox)_3ClWNO$ (**9**) could only be prepared as a mixture. The best results were obtained when a hexane solution of $(silox)_3WCl$ (**6**) was exposed to 3 equiv of NO for 5 min at −78 °C, followed by a rapid removal of excess NO and solvent. A red solid was obtained consisting of 78% **9**, 11% $(silox)_3WCl_2$ (**5**), and 11% $(silox)_3WNO$ (**10**). The IR spectrum of the mixture revealed a strong band at 1651 cm^{-1} attributed to the ν(NO) of **9**, and a weaker absorbance at 1574 cm^{-1} that was assigned to the nitrosyl stretch of **10**.[47]

Synthesis of the tungsten(II) nitrosyl $(silox)_3WNO$ (**10**) was accomplished via addition of Na/Hg to $(silox)_3WCl$ (**6**) in the presence of NO. Since $(silox)_3ClWNO$ (**9**) was likely to be the true target of reduction, this process was complicated by the same side reactions described above, and optimal conditions were found to be 2 equiv of Na/Hg, 2 equiv of NO, and <10 min reaction time in THF. Precipitation from Et_2O afforded **10** in 24% yield as a yellow powder that contained minimal impurities (<5% by ^1H NMR analysis). The 1574 cm^{-1} nitrosyl stretch observed in the IR spectrum of **10** is indicative of significant backbonding from the W(II) center to the NO π*-orbitals. Similar low ν(NO) values have been observed by Legzdins et al.[48] for a number of tungsten(II) nitrosyl complexes of the type Cp*W(NO)(R)(R′) (e.g., R = Me, R′ = tolyl, ν(NO) = 1536 cm^{-1}).

Abstraction of the oxygen atom from $(silox)_3WNO$ (**10**) is a plausible route to $(silox)_3WN$ (**11**), as Cummins et al. have shown via the deoxygenation of $(ArNR)_3CrNO$ by $(Mes)_3V(THF)$ to give $(ArNR)_3CrN$ and $(Mes)_3VO$.[24] Separation difficulties render this route problematic on a preparative scale, so 2-methylaziridine was explored as a N-atom source[49] in order to obtain a pure sample of **11**. Treatment of $(silox)_3WCl$ (**6**) with 2 equiv of $HNCH_2CHMe$ in benzene provided $(silox)_3WN$ (**11**) in 22% yield as a light pink solid that contained <5% $(silox)_3WCl_2$ (**5**). Nitride **11** could be obtained in reasonable analytical purity upon repeated recrystallizations from pentane.

(47) Hayton, T. W.; Legzdins, P.; Sharp, W. B. *Chem. Rev.* **2002**, *102*, 935−991.
(48) (a) Legzdins, P.; Rettig, S. J.; Ross, K. J.; Weltheer, J. E. *J. Am. Chem. Soc.* **1991**, *113*, 4361−4363. (b) Brouwer, E. B.; Legzdins, P.; Rettig, S. J.; Ross, K. J. *Organometallics* **1994**, *13*, 2088−2091. (c) Debad, J. D.; Legzdins, P.; Reina, R.; Young, M. A.; Batchelor, R. J.; Einstein, F. W. B. *Organometallics* **1994**, *13*, 4315−4321.
(49) Mindiola, D. J.; Cummins, C. C. *Angew Chem., Int. Ed.* **1998**, *37*, 945−947.

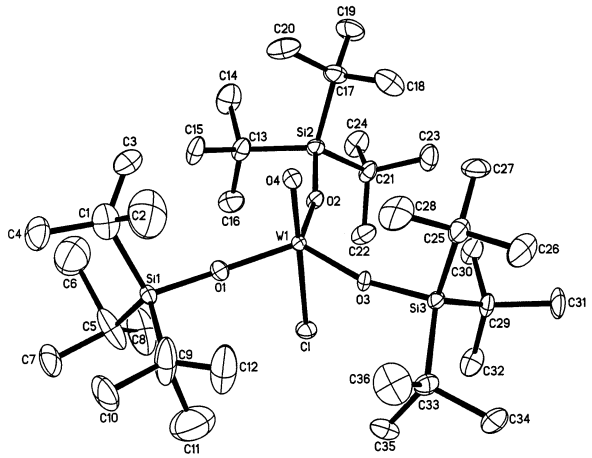

Figure 4. Molecular view (40% ellipsoids) of $(silox)_3ClWO$ (**7**).

Table 6. Selected Interatomic Distances (Å) and Angles (deg) for $(silox)_3ClWO$ (**7**)

W−O4	1.723(6)	W−O1	1.830(6)	W−O2	1.840(5)
W−Cl	2.518(2)	W−O3	1.841(4)		
Si1−O1	1.701(6)	Si2−O2	1.707(6)	Si3−O3	1.700(5)
Si−C_{av}	1.91(2)	C−C_{av}	1.54(5)		
O1−W−O4	95.5(3)	O2−W−O4	95.7(3)	O3−W−O4	96.5(2)
O1−W−Cl	84.0(2)	O2−W−Cl	84.09(19)	O3−W−Cl	84.15(19)
O1−W−O2	118.2(3)	O1−W−O3	120.4(3)	O2−W−O3	118.2(3)
O4−W−Cl	179.3(2)	W−O1−Si1	165.7(4)	W−O2−Si2	161.5(4)
W−O3−Si3	166.6(5)	O−Si−C_{av}	105.6(14)	C−Si−C_{av}	113.0(13)
Si−C−C_{av}	112.0(38)	C−C−C_{av}	106.3(63)		

9. Structure of $(silox)_3ClWO$. Single-crystal X-ray analysis of $(silox)_3ClWO$ (**7**) confirmed its C_{3v}, pseudo-tbp geometry, with the silox groups occupying equatorial positions (Figure 4, Table 2, Table 6). The axial oxo ligand has a somewhat long bond length (vide infra) of 1.723(6) Å,[46] perhaps influenced by the trans-axial chloride, whose d(W−Cl) = 2.5180(19) Å. The tungsten−oxygen bond lengths of the silox ligands are typical (1.837(6) Å (av)), and the O(silox)−W−O(oxo) angles are 95.9(5)°, thereby reflecting the influence of the short, multiply bonded oxo ligand. In contrast, the long tungsten chloride bond accommodates the acute O(silox)−W−Cl angles of 84.08(8)°, while the O(silox)−W−O(silox) angles are only subtly perturbed from trigonal (118.9(13)°).

The faint pink color of the crystal used for the X-ray analysis belied the W(VI) oxidation state of the oxo chloride. A ^{1}H NMR spectrum of the sample from which it was taken indicated the presence of 0.91% $(silox)_3WCl_2$ (**5**), a bright pink W(V) complex. Parkin[50] showed that a molybdenum site containing oxo and chloride is dominated by the latter. From his data, it is estimated that the actual d(WO) in (**7**) is likely to be 0.02−0.04 Å shorter, which brings the bond length into a normal or slightly elongated regime.

Oxygen Atom Transfer Studies. 1. Tungsten. In the original tungsten experiments regarding $(silox)_3WCl$ (**6**) and N_2O or NO, identification of the new products was somewhat problematic because of the lack of common NMR spectroscopic handles, and the minimal chemical shift dispersion pertaining to ^{1}H NMR signals of the silox ligand. Initially, nitride $(silox)_3WN$ (**11**) was considered as a possible product in the reactions, hence alternative routes to the complex were sought.[51]

Once $(silox)_3WNO$ (**10**) was eventually prepared, it was treated with $(silox)_3WCl$ (**6**), but under no conditions was O-atom transfer to give $(silox)_3ClWO$ (**7**) effected. Since the transfer of oxygen from Cl_4WO to PMe_3 is supposed to be thermodynamically favorable by ∼12 kcal/mol,[52] **7** was treated with PMe_3, but upon thermolysis at 100 °C in C_6D_6 for >1 day, no Me_3PO was detected. Failed attempts to effectively deoxygenate **10** to give nitride $(silox)_3WN$ (**11**) prompted a more systematic investigation of O-atom transfers, with $(silox)_3M$ (**1**-M, M = V, NbL (L = 4-pic, PMe_3), Ta) utilized as potential oxygen-atom acceptors.

2. $(silox)_3WNO$ (10) Deoxygenations. The reactivity of $(silox)_3WNO$ (**10**) with $(silox)_3M$ (**1**-M, M = V, NbL (L = 4-pic,[29,53,54] PMe_3), Ta)[30] is summarized in Scheme 2. With vanadium as the O-atom acceptor, deoxygenation of **10** took place rather slowly at 85 °C in benzene-d_6, with a rough rate constant of $k \sim 1.4 \times 10^{-4}$ M^{-1} s^{-1} ($\Delta G^{\ddagger}$(85 °C) ∼ 27 kcal/mol). $(silox)_3Nb$(4-pic) (**1**-Nb-4-pic) also deoxygenated the nitrosyl of **10** under the same conditions (50% after 4 h), but the reaction slowed noticeably with time, implicating inhibition by free 4-picoline. With $(silox)_3NbPMe_3$ (**1**-$NbPMe_3$) as the deoxygenating agent, milder conditions (23 °C, benzene-d_6) were employed, but the observations were similar. Initial deoxygenation products appeared swiftly, but the reaction then slowed beyond that expected for a simple second-order process (61% conversion after 2 days; 86% after 9 days). With 8 equiv of PMe_3 present, only 10% conversion to deoxygenation products was noted after 2 days.

Surprisingly, coordinatively unsaturated $(silox)_3Ta$ (**1**-Ta) was the least effective of the three derivatives. **1**-Ta, which deoxygenates small molecules like CO and NO at <0 °C very rapidly,[29,30] mostly (87%) cyclometalated to $(silox)_2$-$HTaOSi^tBu_2CMe_2CH_2$ (**12**-Ta)[55] with a rough rate constant of $k \sim 5.0 \times 10^{-6}$ s^{-1} (23 °C). About 12% of $(silox)_3WN$ (**11**) and the corresponding tantalum oxo, $(silox)_3TaO$ (**2**-Ta) were observed upon completion, and an appropriate amount of tungsten nitrosyl (**10**) remained. Slightly more deoxygenation (23%) was observed when the reaction was conducted at 85 °C, and upon completion (11 h), the NMR tube was kept in the constant-temperature bath for 65 days and occasionally monitored by ^{1}H NMR spectroscopy. Within experimental error, the ratio of products did not change over the course of time, hence **12**-Ta did not appear to reversibly generate **1**-Ta.

(50) Parkin, G. *Acc. Chem. Res.* **1992**, *25*, 455−460.

(51) (a) Chisholm, M. H.; Hoffman, D. M.; Huffman, J. C. *Inorg. Chem.* **1983**, *22*, 2903−2906. (b) Chisholm, M. H.; Folting, K.; Lynn, M. L.; Tiedtke, D. B.; Lemoigno, F.; Eisenstein, O. *Chem. Eur. J.* **1999**, *5*, 2318−2326. (c) Pollagi, T. P.; Stoner, T. C.; Dallinger, R. F.; Gilbert, T. M.; Hopkins, M. D. *J. Am. Chem. Soc.* **1991**, *113*, 703−704.

(52) Holm, R. H.; Donahue, J. P. *Polyhedron* **1993**, *12*, 571−593.

(53) Covert, K. J.; Neithamer, D. R.; Zonnevylle, M. C.; LaPointe, R. E.; Schaller, C. P.; Wolczanski, P. T. *Inorg. Chem.* **1991**, *30*, 2494−2508.

(54) (a) Kleckley, T. S.; Bennett, J. L.; Wolczanski, P. T.; Lobkovsky, E. B. *J. Am. Chem. Soc.* **1997**, *119*, 247−248. (b) Kleckley, T. S. Ph.D. Thesis, Cornell University, 1998.

(55) Miller, R. L.; Toreki, R.; LaPointe, R. E.; Wolczanski, P. T.; Van Duyne, G. D.; Roe, D. C. *J. Am. Chem. Soc.* **1993**, *115*, 5570−5588.

Scheme 2

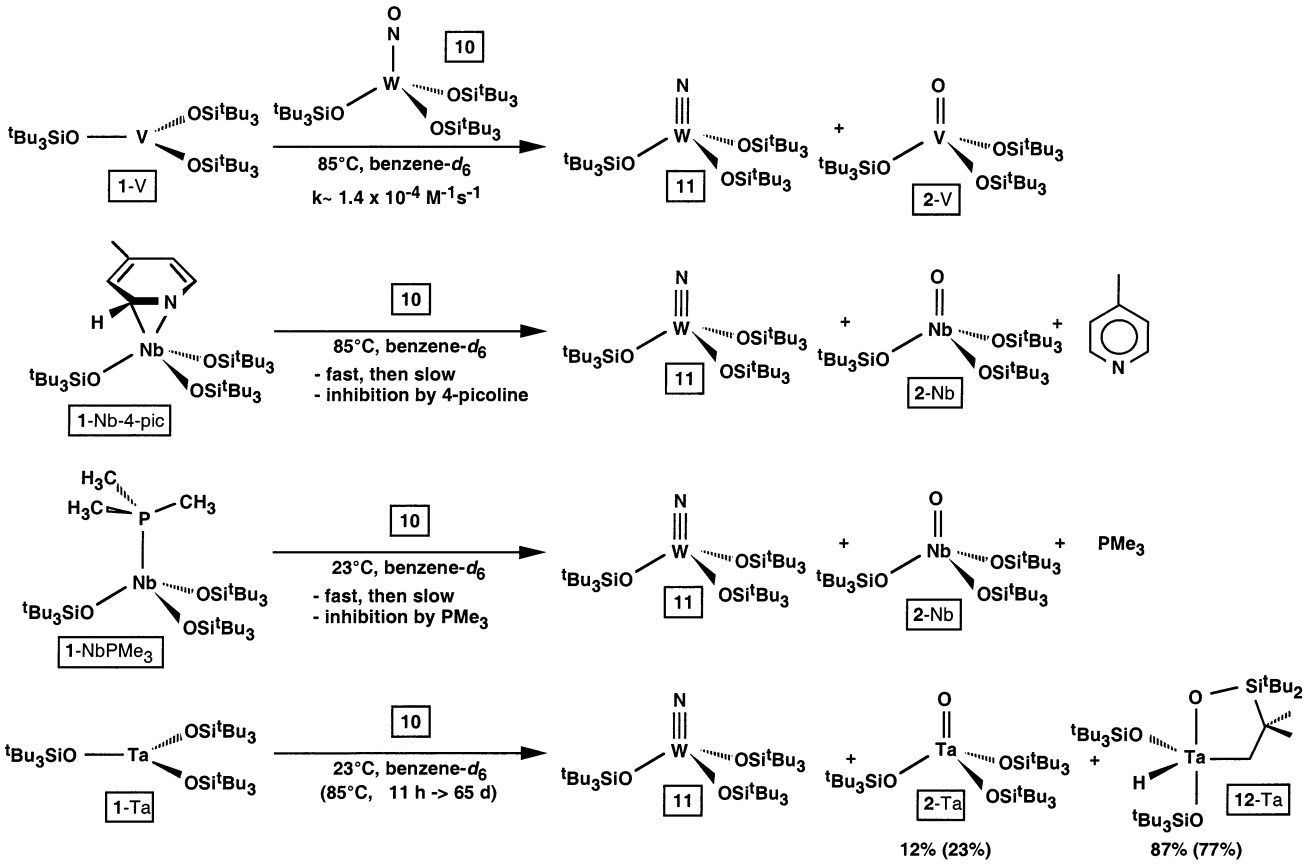

The relative unreactivity of **1**-Ta toward deoxygenation of $(silox)_3WNO$ (**10**) and its proclivity toward binding N-heterocycles[53] suggested that it could be used as a scavenger as indicated in Scheme 3. When **1**-Ta was present along with $(silox)_3Nb$(4-pic) (**1**-4-pic) and **10**, the formation of $(silox)_3Ta$(4-pic) (**1**-Ta-4-pic) occurred swiftly (<5 min) and concomitantly with niobium cyclometalation (>90%) to two isomers of $(silox)_2HNbOSi^tBu_2CMe_2CH_2$ (**12**-Nb) and deoxygenation (<10%) to $(silox)_3NbO$ (**2**-Nb) and $(silox)_3WN$ (**11**). The cyclometalation products **12**-Nb could not be isolated from this reaction, but their spectral signatures are comparable to that of $(silox)_2HTaOSi^tBu_2CMe_2CH_2$ (**12**-Ta)[55] as Table 1 indicates. Furthermore, addition of 4-picoline to the mixture containing **12**-Nb regenerated **1**-Nb-4-pic, and **12**-Nb slowly deoxygenated **10** over the course of days, hence cyclometalation appears reversible. The tantalum scavenging experiment is rationalized as the capture of 4-picoline that dissociates from **1**-Nb-4-pic, or the associative abstraction of 4-picoline by **1**-Ta. Transient $(silox)_3Nb$ (**1**-Nb) then undergoes predominantly first-order cyclometalation in competition with second-order deoxygenation on a time scale too swift to follow by ^{1}H NMR spectroscopy.

3. R_3PO (R = Me, Ph, ^{t}Bu) Deoxygenations. As Scheme 4 illustrates, $(silox)_3V$ (**1**-V) did not effect the deoxygenation of the phosphine oxides, but instead generated the adducts $(silox)_3VOPR_3$ (**3**-OPR$_3$; R = Me, Ph, ^{t}Bu),[56] which could be synthesized in high yield as explained above. Thermolysis of the adducts was ineffective at oxygen removal, and it was shown that $(silox)_3VO$ (**2**-V) and PMe_3 could be very slowly converted (~70%) to $(silox)_3VOPMe_3$ (**3**-OPMe$_3$) over the course of 86 days at 100 °C.[56−60]

For niobium, deoxygenation of R_3PO (R = Me, Ph) by $(silox)_3NbPMe_3$ (**1**-NbPMe$_3$) occurred swiftly (<5 min) under ambient conditions in benzene-d_6, as did the formation of $(silox)_3NbO$ (**2**-Nb) and PMe_3 from $(silox)_3Nb$(4-pic) (**1**-Nb-4-pic) and Me_3PO. When the 4-picoline derivative was used to deoxygenate Ph_3PO, only 50% deoxygenation was observed at <5 min and at 15 h 85% conversion was achieved. Apparently the buildup of 4-picoline during the course of the reaction is enough to inhibit the second-order O-atom transfer process. With ^{t}Bu$_3$PO as the substrate, neither Nb derivative gave products indicative of deoxygenation. At 23 °C in the presence of 10 equiv of ^{t}Bu$_3$PO, **1**-NbPMe$_3$ slowly degraded while the phosphine oxide remained intact. The 4-picoline "masked Nb(III)" species, **1**-Nb-4-pic, can withstand substantial thermolysis, but after

(56) Similar intermediates have recently been identified in transferases: Smith, P. D.; Millar, A. J.; Young, C. G.; Ghosh, A.; Basu, P. *J. Am. Chem. Soc.* **2000**, *122*, 9298−9299.

(57) (a) Espensen, J. H.; Shan, X.; Wang, Y.; Huang, R.; Lahti, D. W.; Dixon, J.; Lente, G.; Ellern, A.; Guzei, I. A. *Inorg. Chem.* **2002**, *41*, 2583−2591. (b) Wang, Y.; Lente, G.; Espensen, J. H.; Guzei, I. A. *Inorg. Chem.* **2002**, *41*, 1272−1280.

(58) Nemyin, v. N.; Divie, S. R.; Mondal, S.; Rubie, N.; Kirk, M. L.; Somogyi, A.; Basu, P. *J. Am. Chem. Soc.* **2002**, *124*, 756−757.

(59) (a) Gangopadhyay, J.; Sengupta, S.; Bhattacharyya, S.; Chakraborty, I.; Chakravorty, A. *Inorg. Chem.* **2002**, *41*, 2616−2622. (b) Bhattacharyya, S.; Chakraborty, I.; Dirghangi, B. K. *Inorg. Chem.* **2001**, *40*, 286−293.

(60) Arias, J.; Newlands, C. R.; Abu-Omar, M. M. *Inorg. Chem.* **2001**, *40*, 2185−2192.

Scheme 3

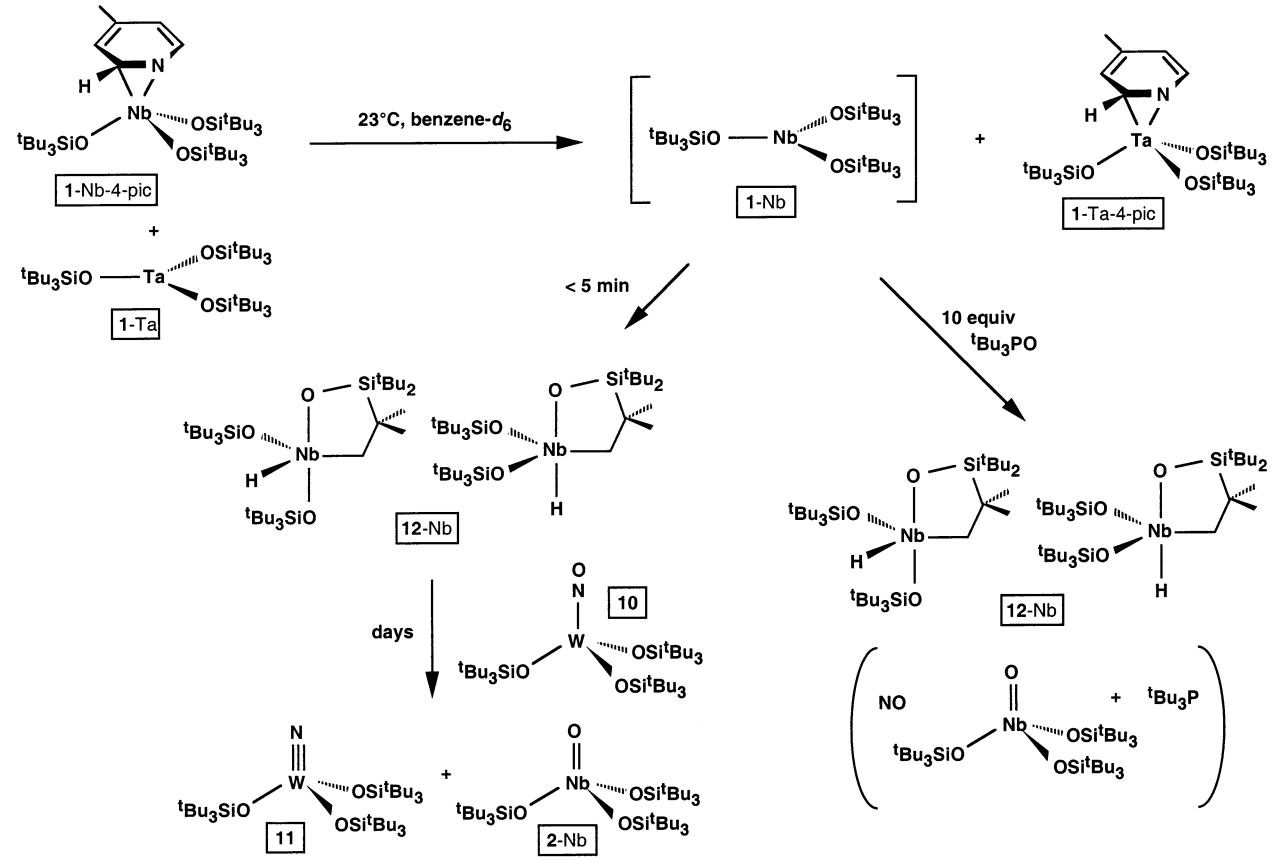

Scheme 4

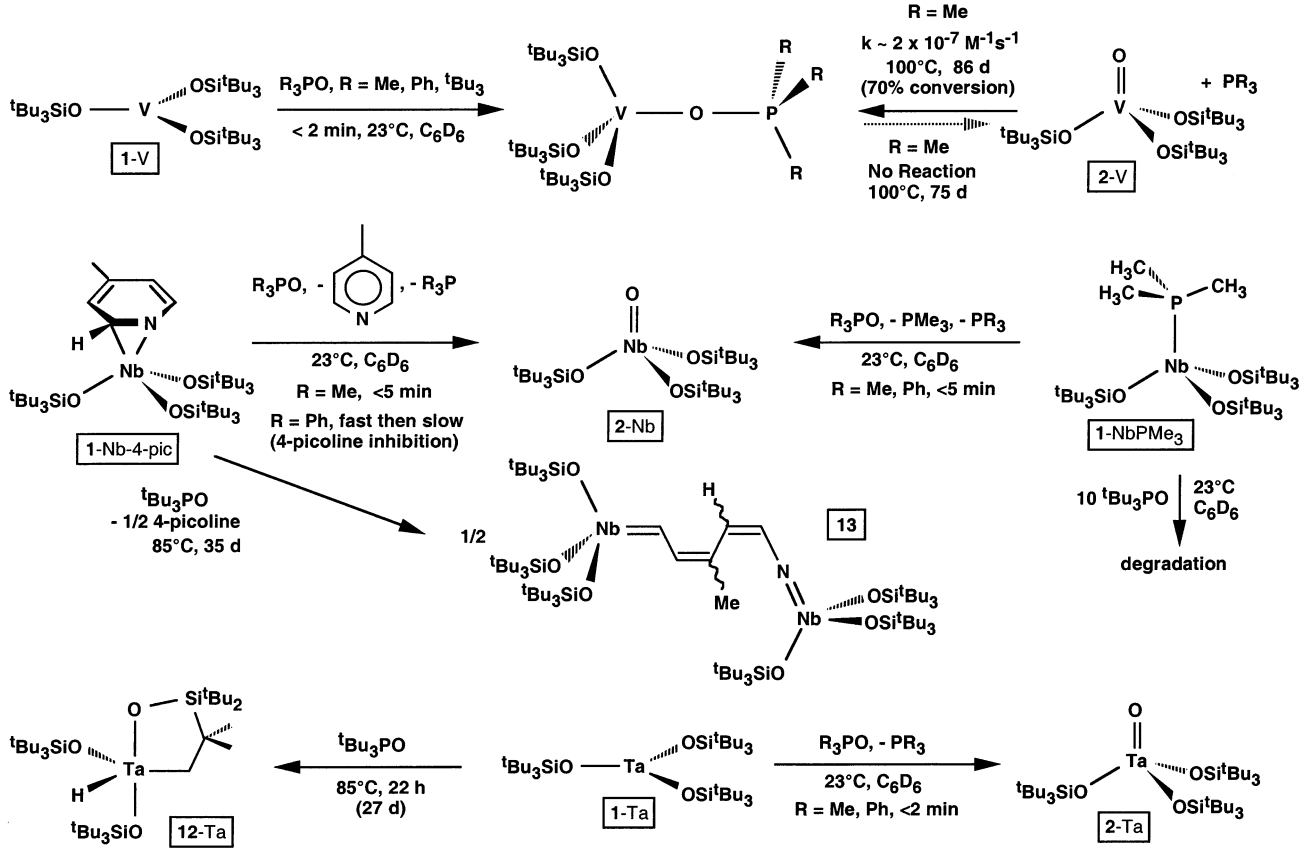

35 days at 85 °C with ^{t}Bu$_3$PO present, the complex failed to induce O-atom transfer. Instead, loss of $^1/_2$ equiv of 4-picoline and ring opening of the heterocycle to (silox)$_3$Nb=CH(*cis*-CH=CMe)(*cis*-CH=CH)N=Nb(silox)$_3$ (**13**) was evident. Although the compound was not isolated, its spectral signature and the stoichiometry of the reaction left little doubt as to its composition. Its stereochemistry is tentatively assigned from comparisons to the related ring-open products of pyridine, 2-picoline, 3-picoline and the stereoisomers of (silox)$_3$Nb=CHCH=CHCH=CHN=Ta(silox)$_3$.[54]

As Scheme 3 shows, even the use of (silox)$_3$Ta (**1**-Ta) as a 4-picoline scavenger did not result in ^{t}Bu$_3$PO deoxygenation by (silox)$_3$Nb(4-pic) (**1**-Nb-4-pic). With 10 equiv of ^{t}Bu$_3$PO present at 23 °C in benzene-d_6, abstraction of 4-picoline from **1**-Nb-4-pic by **1**-Ta afforded (silox)$_3$Ta(4-pic) (**1**-Ta-4-pic) as expected, but the cyclometalation isomers (silox)$_2$HNbOSi^{t}Bu$_2$CMe$_2$CH$_2$ (**12**-Nb) were the only niobium-containing products. If formed, it is clear that an intermediate of the type "(silox)$_3$NbOPR$_3$" cannot deoxygenate when R = ^{t}Bu. Note that the structure of (silox)$_3$VOP^{t}Bu$_3$ (**3**-OP^{t}Bu$_3$) shows that a similar niobium adduct is certainly feasible from a steric standpoint.

As for (silox)$_3$Ta (**1**-Ta), the deoxygenation studies involving R$_3$PO are strikingly similar to the niobium results. Both Me$_3$PO and Ph$_3$PO are deoxygenated rapidly (<2 min) at 23 °C in C$_6$D$_6$, but no O-atom transfer from ^{t}Bu$_3$PO was noted, even at 85 °C, and cyclization to (silox)$_2$-HTaOSi^{t}Bu$_2$CMe$_2$CH$_2$ (**12**-Ta) was observed instead. Prolonged thermolysis (85 °C, 27 days) of the "tuck-in" derivative **12**-Ta in the presence of ^{t}Bu$_3$PO failed to elicit any evidence of reversible cyclometalation, and the phosphine oxide was untouched.

4. Thermochemical Calculations on Deoxygenation. A variety of levels of theory were employed in conjunction with the SBK(d) effective core potential/valence basis sets on model systems where HO was used in place of the ^{t}Bu$_3$SiO ligand.[61−66] For the deoxygenation of (HO)$_3$WNO (**10′**) by (HO)$_3$M (**1′**-M, M = V, Nb, Ta) shown in eq 5, each

$$\underset{\mathbf{10'}}{(HO)_3WNO} + \underset{\mathbf{1'}\text{-M, M = V, Nb, Ta}}{(HO)_3M} \xrightarrow{25\ ^\circ C} \underset{\mathbf{11'}}{(HO)_3WN} + \underset{\mathbf{2'}\text{-M}}{(HO)_3MO} \quad (5)$$

case was determined to be exoergic by a substantial amount. At arguably the highest level of theory, CCSD(T) (coupled clusters with single and double excitations and triples added noniteratively), $\Delta G°$(25 °C, V) = −66 kcal/mol, $\Delta G°$(Nb) = −100 kcal/mol, and $\Delta G°$(Ta) = −100 kcal/mol. Considerably greater variation in vanadium (see Experimental Section) was evidenced in comparison to Nb and Ta, whose free energies for eq 5 were remarkably close (standard deviation less than 15 kcal/mol at all correlated levels).

Calculational aspects of phosphine oxide deoxygenation were not explored as extensively as the nitrosyl case, and only Me$_3$PO was examined, as illustrated in eq 6. The

$$Me_3PO + \underset{\mathbf{1'}\text{-M, M = V, Nb, Ta}}{(HO)_3M} \xrightarrow{25\ ^\circ C} Me_3P + \underset{\mathbf{2'}\text{-M}}{(HO)_3MO} \quad (6)$$

electronic differences between the phosphines of interest were not deemed to be significant enough to warrant exhaustive examination. Since Me$_3$PO was estimated to be more difficult than Ph$_3$PO by ∼6 kcal/mol,[52] and was the simplest of the three, it was used in the study. For M = Nb and Ta, the deoxygenation of Me$_3$PO was calculated to be exoergic, with $\Delta G°$(Nb) ∼ $\Delta G°$(Ta) = −45 kcal/mol. For vanadium, eq 6 was calculated to be only −15 kcal/mol exoergic, and the observed stability of (silox)$_3$VOPR$_3$ (**3**-OPR$_3$, R = Me, Ph, ^{t}Bu) was of some concern. As a consequence, the formation of (HO)$_3$VOPMe$_3$ (**3′**-OPMe$_3$) from **1′**-V and Me$_3$PO was also calculated, as eq 7 reveals, and its $\Delta G°$ of −20 kcal/

$$Me_3PO + \underset{\mathbf{1'}\text{-V}}{(HO)_3V} \xrightarrow{25\ ^\circ C} \underset{\mathbf{3'}\text{-OPMe}_3}{(HO)_3VOPMe_3} \quad (7)$$

mol concurred with experiment; the adduct was the most stable entity in the vanadium system.

Calculations on the thermochemistry arising from deoxygenation of Cl$_4$WO by PH$_3$ (∼+50 kcal/mol) or PMe$_3$ (∼+40 kcal/mol) were extremely endoergic, in direct conflict with experimental data.[52] In addition, a significant degree of variation in the calculations was experienced when calibration of other O-atom transfers involving WCl$_4$ and PMe$_3$ was conducted. As a consequence, the O-atom transfer chemistry of the tungsten complexes—or lack thereof—was set aside until further experiments and more accurate calculations could be done.

Discussion

Coordination Complexes. The new coordination complexes described herein are relatively unexceptional given previous studies, but a few derivatives are worth comment. The Nb(III) derivative, (silox)$_3$NbPMe$_3$ (**1**-NbPMe$_3$), is a rare monomeric example of this uncommon oxidation state.[41,42] While it is tempting to conclude that its distorted tetrahedral geometry, which approaches that of a trigonal monopyramid,[67] is a natural consequence of the severe steric constraints

(61) Stevens, W. J.; Krauss, M.; Basch, H.; Jasien, P. G. *Can. J. Chem.* **1992**, *70*, 612−630.
(62) Benson, M. T.; Cundari, T. R.; Lutz, M. L.; Sommerer, S. O. In *Reviews in Computational Chemistry*; Boyd, D., Lipkowitz, K., Eds.; Wiley: New York, 1996; Vol. 8, p 145.
(63) Becke, A. D. *J. Chem. Phys.* **1993**, *98*, 5648−5652.
(64) Bartlett, R. J.; Stanton, J. F. In *Reviews in Computational Chemistry*; Boyd, D. B., Lipkowitz, K. B., Eds.; Wiley: New York, 1994; Vol. 5, pp 65−169.
(65) Frenking, G.; Antes, I.; Bohme, M.; Dapprich, S.; Ehlers, A. W.; Jonas, V.; Neuhaus, A.; Otto, M.; Stegmann, R.; Veldkamp, A.; Vyboishchikov, S. F. In *Reviews in Computational Chemistry*; Boyd, D., Lipkowitz, K., Eds.; Wiley: New York, 1996; Vol. 8, pp 63−144.
(66) Frisch, M. J.; Trucks, G. W.; Schlegel, H. B.; Scuseria, G. E.; Robb, M. A. Cheeseman, J. R.; Zakrzewski, V. G.; Montgomery, J. A., Jr.; Stratmann, R. E.; Burant, J. C.; Dapprich, S.; Millam, J. M.; Daniels, A. D.; Kudin, K. N.; Strain, M. C.; Farkas, O.; Tomasi, J.; Barone, V.; Cossi, M.; Cammi, R.; Mennucci, B.; Pomelli, C.; Adamo, C.; Clifford, S.; Ochterski, J.; Petersson, G. A.; Ayala, P. Y.; Cui, Q., Morokuma, K.; Malick, D. K.; Rabuck, A. D.; Raghavachari, K.; Foresman, J. B.; Cioslowski, J.; Ortiz, J. V.; Stefanov, B. B.; Liu, G.; Liashenko, A.; Piskorz, P.; Komaromi, I.; Gomperts, R.; Martin, R. L.; Fox, D. J.; Keith, T.; Al-Laham, M. A.; Peng, C. Y.; Nanayakkara, A.; Gonzalez, C.; Challacombe, M.; Gill, P. M. W.; Johnson, B.; Chen, W.; Wong, M. W.; Andres, J. L.; Gonzalez, C.; Head-Gordon, M.; Replogle, E. S.; Pople, J. A. Gaussian, Inc.; Pittsburgh, PA, 1998.

imposed by the silox groups, the PMe_3 ligand actually has a substantially larger cone angle.[68] An increase in the O(pπ)→Nb(dπ) interactions as the O_3Nb core approaches a trigonal planar geometry may help offset the phosphine/silox sterics, which are also somewhat alleviated by the subtle canting of the Nb−O−Si linkages.

Both tungsten oxo derivatives prepared during the course of these studies are unusual. The C_{3v} geometry of $(silox)_3ClWO$ (**7**) is uncommon, in part because it contains an axial oxo ligand directly opposite another fairly strong π-donor, the chloride. The elongation of d(W−Cl) by ∼0.15 Å relative to that of $(silox)_3WCl_2$ (**5**) is a testament to the trans influence of the oxo ligand, whose much shorter bond distance permits it to exert a greater repulsive effect on the silox oxygens, resulting in a slight cant of the siloxides toward the chloride.[46] $(silox)_3WO$ (**8**), which is likely to possess a pseudotetrahedral C_{3v} structure, is a rare example of a tungsten(V) oxo derivative; most WO species are either W(VI) or W(IV). Unfortunately, efforts at crystallographic characterization of **8** or the related $(silox)_3TaO$ (**2**-Ta) were not successful.

$(silox)_3WNO$ (10) Deoxygenations. 1. Relative Rates. Even allowing for calculational inaccuracies, there can be no question that the deoxygenation of $(silox)_3WNO$ (**10**) by $(silox)_3M$ (**1**-M, M = V, Nb, Ta) is greatly thermodynamically favorable. From the standpoint of a possible linear free energy relationship, the rates of deoxygenation should follow the trend Ta ∼ Nb > V. Moreover, simple atom transfers that are −65 kcal/mol (V) and −100 kcal/mol (Nb, Ta) exoergic would normally be exceedingly swift.

Niobium appears to deoxygenate **10** the swiftest, although the process is complicated by the apparent inhibition by released ligand, since $(silox)_3Nb$ (**1**-Nb) is only stable as an adduct, $(silox)_3NbL$ (**1**-NbL). Two mechanisms for L (L = 4-picoline, PMe_3) inhibition seem plausible. In the first, L dissociation occurs to provide **1**-Nb, which can either recapture L or attack **10** and proceed to deoxygenate (eqs 8, 10−12). The rate expression for this scenario is −d[**1**-NbL]/

$$\underset{\textbf{1}\text{-NbL}}{(silox)_3NbL} \underset{k_{-1}}{\overset{k_1}{\rightleftharpoons}} \underset{\textbf{1}\text{-Nb}}{(silox)_3Nb} + L \quad (8)$$

$$\underset{\textbf{1}\text{-NbL}}{(silox)_3NbL} + \underset{\textbf{10}}{(silox)_3WNO} \underset{k'_{-1}}{\overset{k'_1}{\rightleftharpoons}} \underset{\textbf{1}\text{-Nb-}\textbf{10}}{(silox)_3Nb\text{-}ONW(silox)_3} + L \quad (9)$$

$$\underset{\textbf{1}\text{-M, M = V, Nb, Ta}}{(silox)_3M} + \underset{\textbf{10}}{(silox)_3WNO} \underset{k_{-a}}{\overset{k_a}{\rightleftharpoons}} \underset{\textbf{1}\text{-M-}\textbf{10}\text{ (precursor)}}{(silox)_3M\text{-}ONW(silox)_3} \quad (10)$$

$$\underset{\textbf{1}\text{-M-}\textbf{10}\text{, M = V, Nb, Ta}}{(silox)_3M\text{-}ONW(silox)_3} \xrightarrow{k_t} \underset{\textbf{2}\text{-M-}\textbf{11}\text{ (successor)}}{(silox)_3MO\text{-}NW(silox)_3} \quad (11)$$

$$\underset{\textbf{2}\text{-M-}\textbf{11}\text{, M = V, Nb, Ta}}{(silox)_3MO\text{-}NW(silox)_3} \xrightarrow{fast} \underset{\textbf{2}\text{-M}}{(silox)_3MO} + \underset{\textbf{11}}{(silox)_3WN} \quad (12)$$

$dt = k_1k_ak_t[\textbf{1}\text{-NbL}][\textbf{10}]/\{(k_{-1}k_{-a} + k_{-1}k_t)[L] + k_ak_t[\textbf{10}]\}$, which leads to the simplification $-d[\textbf{1}\text{-NbL}]/dt = k_1k_ak_t[\textbf{1}\text{-NbL}][\textbf{10}]/\{(k_{-1}k_{-a} + k_{-1}k_t)[L]\}$ when $(k_{-1}k_{-a} + k_{-1}k_t)[L]$ is consequential, and quite plausibly $-d[\textbf{1}\text{-NbL}]/dt = k_1k_ak_t[\textbf{1}\text{-NbL}][\textbf{10}]/k_{-1}k_{-a}[L]$ if O-atom transfer is rate determining. As Scheme 3 reveals, when **1**-Nb is generated, deoxygenation of **10** is uncompetitive with cyclometalation, hence eqs 8 and 9 cannot be operational for **1**-$NbPMe_3$. Although this path is not probable for **1**-Nb-4-pic either, it cannot be ruled out since deoxygenations with **1**-Nb-4-pic were conducted at 85 °C, and 4-pic was shown to convert **12**-Nb to the picoline adduct.

In a more probable alternative sequence, **10** displaces L from **1**-Nb to afford the precursor complex $(silox)_3Nb\text{-}ONW(silox)_3$ (**1**-Nb-**10**, eq 9), which then transfers oxygen in the rate-determining step (eq 11) and fragments (eq 12). Here the rate expression is $-d[\textbf{1}\text{-NbL}]/dt = k'_1k_t[\textbf{1}\text{-NbL}][\textbf{10}]/(k'_{-1}[L] + k_t)$, which would simplify to $-d[\textbf{1}\text{-NbL}]/dt = k'_1k_t[\textbf{1}\text{-NbL}][\textbf{10}]/k'_{-1}[L]$ when the concentration of [L] is appreciable. Either mechanism reveals an inhibition by [L] as it accumulates as a byproduct in the deoxygenation. There is an additional complication in the case of **1**-Nb-4-pic deoxygenation, because the released 4-picoline also binds reversibly to $(silox)_3WNO$, which could also be inhibiting deoxygenation. The binding has been independently confirmed.

Because of the involvement of L in the niobium experiments, it is difficult to estimate a rate for comparison to the vanadium and tantalum cases. For the sake of further argument, assume the associative path for niobium, with eqs 9,10, and 12 operable and O-atom transfer rate determining. Using $(silox)_3Nb(4\text{-pic})$ (**1**-Nb-4-pic), the rough half-life of 4 h (85 °C, [**1**-Nb-4-pic] = [**10**]) provides a crude rate of $k_{obs}(Nb) \sim 1.4 \times 10^{-3}\ M^{-1}\ s^{-1}$, which includes a preequilibrium factor $k'_1/k'_{-1}[L]$ that is not applicable to the vanadium or tantalum examples. Since ∼2% of $(silox)_3Nb\text{-}ONW(silox)_3$ (**1**-Nb-**10**) would probably be observable by NMR spectroscopy, the preequilibrium can be factored out as roughly <0.02, and $k_{obs}(Nb)$ can be estimated as $>7 \times 10^{-2}\ M^{-1}\ s^{-1}$. Likewise, the half-life of the deoxygenation of **10** involving $(silox)_3NbPMe_3$ (**1**-$NbPMe_3$) at 23 °C led to an estimate of its rate as $\sim 2 \times 10^{-4}\ M^{-1}\ s^{-1}$ (roughly $1 \times 10^{-2}\ M^{-1}\ s^{-1}$ at 85 °C), consistent with the above arguments. By again factoring out the preequilibrium, a final estimate of $>0.5\ M^{-1}\ s^{-1}$ for **1**-$NbPMe_3$ loss is obtained at 85 °C.

For the vanadium case, eqs 10−12 presumably apply, and $k_{obs}(85\ °C) = (k_a/k_{-a})k_t$ from simplification of the rate expression $k_ak_t[\textbf{1}\text{-V}][\textbf{10}]/(k_{-a} + k_t)$, where $k_{-a} \gg k_t$. The rate is approximately $1.4 \times 10^{-4}\ M^{-1}\ s^{-1}$ as determined from the half-life. The same situation applies for tantalum, but cyclometalation interferes and is the major pathway when $(silox)_3Ta$ (**1**-Ta) and $(silox)_3WNO$ (**10**) are combined. By using the cyclometalation rate at 85 °C ($\sim 2.8 \times 10^{-3}\ s^{-1}$) and assuming pseudo-first-order conditions for deoxygen-

(67) Veige, A. S.; Wolczanski, P. T.; Lobkovsky, E. B. *Chem. Commun.* **2001**, 2734−2735.
(68) (a) Tolman, C. A. *Chem. Rev.* **1977**, *77*, 313−348. (b) Bunten, K. A.; Chen, L.; Fernandez, A. L.; Poë, A. J. *Coord. Chem. Rev.* **2002**, *233*−*234*, 41−51.

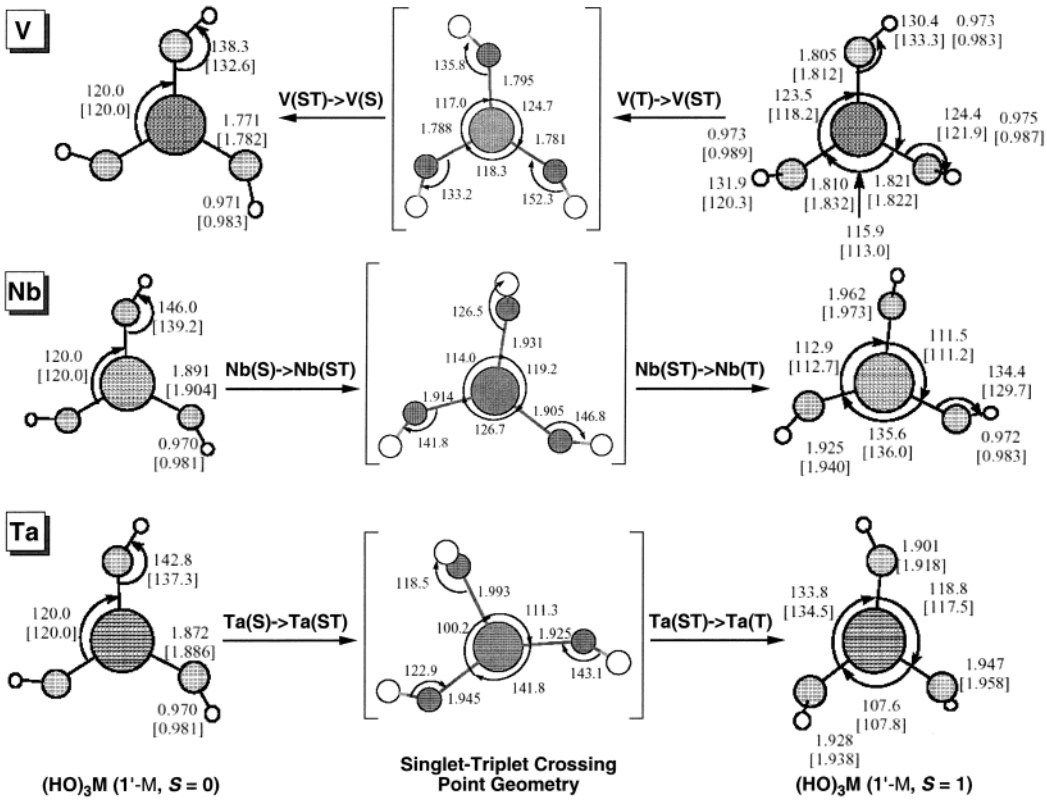

Figure 5. B3LYP/SBK(d) and BLYP/SBK(d) geometries (brackets) of model complexes $(HO)_3M$ (**1′**-M, M = V, Nb, Ta; $S = 0, 1$; Å and deg) and their singlet/triplet crossing points.

ation at early conversion, the crude estimate of the tantalum k_{obs} for deoxygenation is 2×10^{-2} M^{-1} s^{-1}.

In summary, the rough relative rates of deoxygenation for eqs 10 and 11 are Nb ($k_{rel} > 3500$) > Ta (150) > V (1), which is somewhat in line with that postulated on the basis of a linear free energy relationship. Upon closer inspection, though, the situation is less satisfying. It is certainly likely that Nb is substantially greater than the estimation, since $(silox)_3$NbL (**1**-NbL) must lose L to form the precursor complex $(silox)_3$Nb-ONW$(silox)_3$ (**1**-Nb-**10**). Why then are the rates of Nb and Ta so different, and what factors are causing the rates for a single atom transfer with −65 (V) to −100 (Nb, Ta) kcal/mol driving force to occur so slowly?

2. Electronic States of $(silox)_3$M (1-M, M = V, Nb, Ta). Historically, atom transfer is separated into the three steps described by eqs 10−12.[69] The first, docking of the substrate to form the precursor complex, is given by eq 10. O-atom transfer to give the successor complex is given by eq 11, and dissociation of the successor species to product fragments is typically believed to be kinetically inconsequential (eq 12). Immediately, one reason for slow deoxygenation with tantalum becomes apparent. Unlike $(silox)_3$V (**1**-V), which forms adducts with a variety of donors, $(silox)_3$Ta (**1**-Ta) does not incur dative bonding. **1**-V is a ground-state triplet ($S = 1$), and in its probable $(d_{z^2})^1(d_{xz}d_{yz})^1$ configuration ($^3E''$), the d_{z^2} orbital can more readily engage in dative bonding to afford C_{3v} $^3A_2$ $(silox)_3$VL (**1**-VL), with a pair of electrons in the $d_{xz}d_{yz}$ orbital set. **1**-Ta is a ground-state singlet ($S = 0$, $^1A_1'$), and the $(d_{z^2})^2$ configuration is repulsive toward potential donors, as has been previously described.[53] What is the disposition of niobium?

In order to elaborate on the potentially consequential states of $(silox)_3$M (**1**-M, M = V, Nb, Ta), high-level quantum calculations were performed on both singlet and triplet configurations of $(HO)_3$M (**1′**-M, M = V, Nb, Ta; $S = 0, 1$) to probe the energetics. Calculations on singlet and triplet **1′**-M were performed initially with RHF and ROHF wave functions,[70] respectively, to probe the different conformations arising from M−O torsion. As expected, their energetic differences were very small (<1 kcal/mol), and the lowest conformations were then submitted to full B3LYP/SBK(d) and BLYP/SBK(d) geometry optimizations to yield the singlet−triplet energy differences that are tabulated in the Experimental Section.[61−66]

The geometries of $(HO)_3$M (**1′**-M, M = V, Nb, Ta; $S = 0, 1$) are illustrated in Figure 5, and some striking differences are apparent. All of the singlet geometries are trigonal—ignoring HOM linkages—and the metal−oxygen bond distances are relatively normal. The 1.872 Å distance accorded d(Ta−O) is slightly short for silox derivatives,[30,31,53−55,67,71] but there is a lack of true Ta(III) derivatives for ready comparison, hence the available data mostly corresponds to Ta(V) species that are higher coordinate. It is also difficult

(69) (a) Lappin, A. G. *Redox Mechanisms in Inorganic Chemistry*; Ellis Horwood: New York, 1994. (b) Tobe, M. L.; Burgess, J. *Inorganic Reaction Mechanisms*; Addison-Wesley Longman: New York, 1999.

(70) RHF = restricted Hartree−Fock; ROHF = restricted open-shell Hartree−Fock. Young, D. In *Computational Chemistry*; Wiley: New York, 2001; pp 20, 227−229.

(71) Wolczanski, P. T. *Polyhedron* **1995**, *14*, 3335−3362.

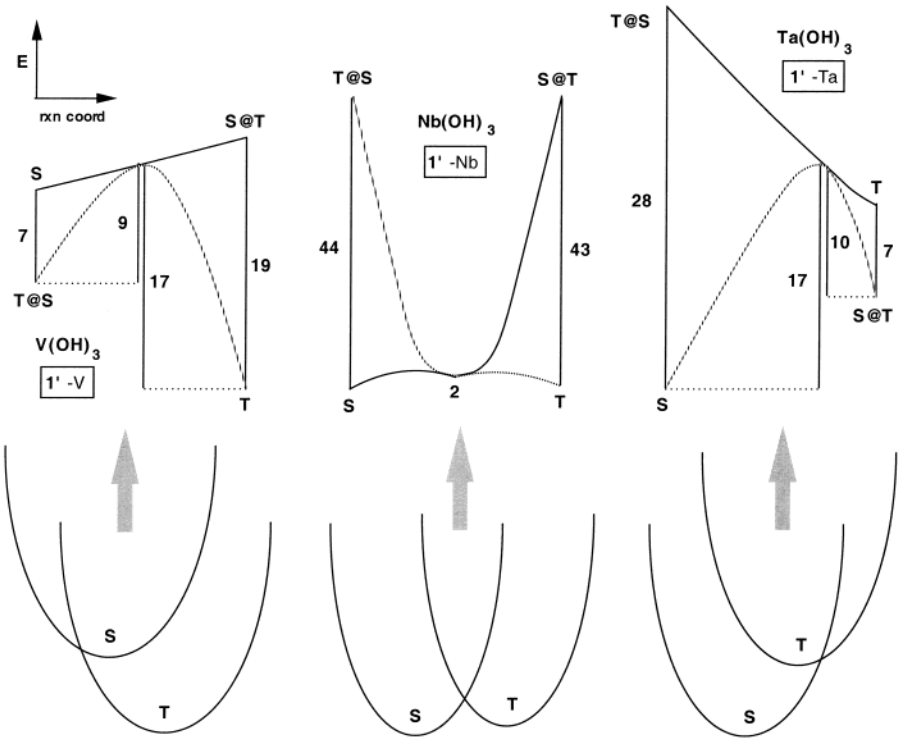

Figure 6. Energetics (kcal/mol, 25 °C) of $(HO)_3M$ (**1′**-M, M = V, Nb, Ta) as models for $(silox)_3M$ (M = V, **1**-V; Nb, **1**-Nb; Ta, **1**-Ta). S and T refer to the singlet and triplet energies at those optimized geometries. S@T refers to the singlet energy at the optimized triplet geometry, and vice versa. Singlet/triplet crossing barriers are indicated by the middle solid vertical lines.

to assess what amount of lengthening could be attributable to steric factors of the silox groups. Nonetheless, the *d*(Nb−O) of 1.891 Å is also slightly short, and $(HO)_3V$ (**1′**-V, *S* = 0) contains vanadium−oxygen bonds that are 1.771 Å, in line with the shorter covalent radius of the first-row element.

The geometries of the triplet configurations are irregular. $(HO)_3V$ (**1′**-V, *S* = 1) exhibits a slight pyramidalization ($\sum\angle$O−M−O = 364°) accompanied by a modest shift toward a Y-shape, while the triplet geometries of **1′**-Nb (*S* = 1) and **1′**-Ta (*S* = 1) distort toward a T-shape ($\sum\angle$O−M−O = 360°). For **1′**-V (*S* = 1), two angles (123.5° and 124.4°) are larger than the third (115.9°), and the *d*(V−O) of 1.81 Å (av) represents a subtle, but real elongation versus the singlet. The magnitude of the distortions is greater for the second- and third-row congeners. For **1′**-Nb (*S* = 1), the 135.6° O−Nb−O angle is much greater than the remaining set (111.5° and 112.9°), and the Nb−O bond (1.962 Å) opposite the largest ∠O−Nb−O is longer than the remaining two (1.925, 1.930 Å), while all are elongated relative to their singlet partners. In **1′**-Ta (*S* = 1), the 133.8° O−Ta−O angle is significantly larger than its 118.8° and 107.6° partners, the Ta−O bond (1.947 Å) opposite the largest ∠O−Ta−O is longer than the others (1.928, 1.901 Å), and all are long relative to the corresponding singlet. Occupation of the metal−oxygen π*-orbital has the expected consequence of increasing *d*(M−O), and in combination with Jahn−Teller distortions, etc., the geometries of the triplet states are readily rationalized.

At all levels of theory from Hartree−Fock to CCSD(T), $(HO)_3V$ (**1′**-V) is predicted to possess a triplet ground state, as illustrated in Figure 6. For levels of theory that include some account of electron correlation, the S−T splitting is fairly consistent at 15(2) kcal/mol. For $(HO)_3Ta$ (**1′**-Ta), a singlet ground state is indicated at all levels of theory above Hartree−Fock (ΔG_{S-T}(av) = −14(1) kcal/mol for all correlated levels of theory). For the niobium congener, $(HO)_3Nb$ (**1′**-Nb), the singlet−triplet energy difference is considerably smaller, with ΔG_{S-T} ranging from 3.9 to −1.4 kcal/mol. The slight preference for a triplet derives mostly from the enthalpic and entropic corrections to the singlet state. Interestingly, the singlet state is preferred (−1.4 kcal/mol) at the CCSD(T)/SBK(d)//B3LYP/SBK(d) level of theory, which is arguably the most accurate in these instances. Apparently the $d_{z^2}/(d_{xz}d_{yz})$ orbital energy difference for V is considerably smaller than its pairing energy, while the related gap for Ta is much larger, leading to its singlet ground state. For niobium, the orbital energy gap and pairing energy must be very similar. The second- and third-row species have greater field strengths and correspondingly greater radial distribution than the vanadium complex, hence their differences are easily rationalized.[38] The difference in behavior between Nb and Ta is less easily explained, since the lanthanide contraction leads to similar radii. Natural bond order calculations on $^1Nb(HO)_3$ (^{1}**1′**-Nb) and $^1Ta(HO)_3$ (^{1}**1′**-Ta) indicate that $5d_{z^2}/6s$ mixing for the latter is greater than the corresponding $4d_{z^2}/5s$ mixing accorded the former. This is also the case for the gas-phase neutral metals.[72] Relativistic effects are an important factor in energetically lowering the more penetrating 6s orbital to improve mixing with $5d_{z^2}$,

(72) Oxtoby, D. W.; Gillis, H. P.; Nachtrieb, N. H. *Principles of Modern Chemistry*, 5th ed.; Thomson Brooks/Cole: U.S.A., 2002; p 552.

thereby minimizing its torus, and providing a much larger $d_{z^2}/(d_{xz}d_{yz})$ energy gap than in the niobium case.

The singlet−triplet (S−T) crossing points for $(HO)_3M$ (**1′**-M; M = V, Nb, Ta) were determined at the B3LYP/SBK(d) level of theory, and their geometries are shown in Figure 5. The crossing point is the geometry at which the singlet and triplet states of **1′**-M are degenerate, and can be considered as a "transition state" connecting the two surfaces, assuming intersystem crossing is probable.[34,35,73,74] To complement these calculations, the energies of the singlet state of **1′**-M at the optimized triplet geometry (S@T), and its triplet state at the optimized singlet geometry (T@S), were also determined in order to construct the free energy vs reaction coordinate diagram illustrated in Figure 6.

For $(HO)_3V$ (**1′**-V), the $S = 1$ state is the ground state with the singlet state about 15 kcal/mol above it. Interestingly, the triplet state is still ∼7 kcal/mol lower than the $S = 0$ state at the optimized geometry of the latter, and the S−T crossing point is only 2 kcal/mol above the singlet geometry. The singlet state does not appear to be very sensitive to geometry, changing only by ∼4 kcal/mol in smoothly traversing from its optimized geometry to that of the triplet. The S−T crossing point geometry reflects its position in the reaction coordinate, with *d*(V−O) intermediate between the singlet and triplet values, and a modest angular change in which the Y-shape of the $S = 1$ state transitions to a T-shape before becoming trigonal at the $S = 0$ state.

In the tantalum case, the situation is reversed from vanadium, and the energy changes are more significant, as expected for the third-row species. The S−T crossing point is proximate to the optimized triplet state along the reaction coordinate and only 3 kcal/mol above it. Bond distances for the S−T crossing point are within error of the $S = 1$ state, but its T-shaped geometry is more evident, with one angle of 142° opposed by an oddly long *d*(Ta−O) of 1.99 Å. The S−T crossing point lies 17 kcal/mol above the $S = 0$ ground state, and now the singlet state is still ∼7 kcal/mol lower than the triplet at the optimized geometry of the latter. The triplet surface is ∼28 kcal/mol above the optimized singlet conformation, and is reasonably consistent with the spectroscopy of $(silox)_3Ta$ (**1**-Ta).[53] The lowest energy absorption band associated with **1**-Ta occurs at 928 nm ($\epsilon = 34$ cm^{-1} M^{-1}, 11900 cm^{-1}), and was tentatively assigned as a $^1A_1' \rightarrow {}^3E''$ transition corresponding to $a_1'^2 \rightarrow a_1'^1e''^1$. This band is accompanied by a similar one at higher energy (612 nm, 16300 cm^{-1}), and both have shoulders. The lower energy band corresponds to ∼31 kcal/mol, which is conspicuously close to the calculated T@S configuration. It is possible that two triplet states arising from Jahn−Teller distortion of the formally D_{3h} $^3E''$ state are manifested by the 928 and 612 nm bands, and the lowest of those is energetically related to the $S = 1$ state of the model complex **1′**-Ta.

$(HO)_3Nb$ (**1′**-Nb) is the most interesting of the three. At the B3LYP/SBK(d) level of theory the triplet is ∼1 kcal/mol lower than the singlet state, and the S−T crossing point is only ∼2 kcal/mol above these states and possesses a geometry that has an intermediate *d*(Nb−O) with a modest T-shaped distortion. As one would expect in this situation, the S@T and T@S energies are 43 and 44 kcal/mol above the respective $S = 1$ and $S = 0$ states. As Figure 6 shows, these high energies and the low-energy S−T crossing point are a consequence of two energetically close states with a modest geometric (i.e., reaction coordinate) difference.

3. Consequences of $(HO)_3M$ (1′-M, M = V, Nb, Ta) Electronic States on Deoxygenation. The thermochemistry for $(silox)_3WNO$ (**10**) deoxygenation, modeled as $(HO)_3WNO$ (**10′**), was broken down into three steps. In eq 13, the energy required to convert singlet $^1M(OH)_3$ (^{1}**1′**-M) to triplet $^3M(OH)_3$ (^{3}**1′**-M) is assessed, followed by deoxygenation to give singlet nitride $^1W(OH)_3N$ (**11′**) and triplet oxo $^3M(OH)_3O$ (^{3}**2′**-M, eq 14), and relaxation of the oxo to its singlet state (**2′**-M, eq 15). At the CCSD(T)/SBK(d)//B3LYP/SBK(d) level of theory, the calculations predict that ^{3}**1′**-Nb and ^{3}**1′**-Ta require 1 and 17 kcal/mol of free energy to be formed from their respective ground state singlets (only at this level of theory is the niobium ground state predicted to be $S = 0$). The deoxygenation step occurs as expected from periodicity, with tantalum (−39 kcal/mol) more exoergic than niobium (−23 kcal/mol), which is more exoergic than vanadium (−18 kcal/mol). It is interesting to note that the greater free energy change for tantalum over niobium compensates for the "activation" of its triplet state, because the relaxation of the oxo triplets to their ground-state singlets is −78 kcal/mol for both metals; relaxation to the singlet state for vanadium oxo is −48 kcal/mol. Together (eqs 13−15), the deoxygenations are −66 kcal/mol exoergic for V, and −100 kcal/mol for Nb and Ta, as espoused above.

$$\underset{^3\mathbf{1'}\text{-M, M = V, Nb, Ta}}{^1M(OH)_3} \xrightarrow{25\ ^\circ C} \underset{^3\mathbf{1'}\text{-M}}{^3M(OH)_3} \qquad (13)$$

$$\underset{\mathbf{10'}}{(HO)_3WNO} + \underset{^3\mathbf{1'}\text{-M, M = V, Nb, Ta}}{^3M(OH)_3} \xrightarrow{25\ ^\circ C} \underset{\mathbf{11'}}{(HO)_3WN} + \underset{^3\mathbf{2'}\text{-M}}{^3M(OH)_3O} \qquad (14)$$

$$\underset{^3\mathbf{2'}\text{-M, M = V, Nb, Ta}}{^3M(OH)_3O} \xrightarrow{25\ ^\circ C} \underset{^3\mathbf{2'}\text{-M}}{^1M(OH)_3O} \qquad (15)$$

Docking of the substrate clearly hampers ready deoxygenation by $(silox)_3Ta$ (**1**-Ta), and inhibition by L (L = PMe_3, 4-pic) is apparent in deoxygenations by $(silox)_3NbL$ (**1**-NbL), yet some critical questions remain. Why is deoxygenation by $(silox)_3V$ so slow if the reaction is exoergic by −66 kcal/mol? Why does rebinding of L compete with deoxygenation by $(silox)_3Nb$ (**1**-Nb) when the latter event is favorable by −100 kcal/mol?

(73) S−T crossing calculations conducted via methods of Harvey, J. N., University of Bristol; personal communication. The use of B3LYP and BLYP functionals does not result in significant changes in the S−T splitting energies or geometries of $M(OH)_3$ (**1′**-M, M = V, Nb, Ta).

(74) (a) Harvey, J. N. In *Spin Forbidden Reactions in Transition Metal Chemistry*; Cundari, T. R., Ed.; Marcel Dekker: Basel, 2001. (b) Harvey, J. N. *J. Am. Chem. Soc.* **2000**, *122*, 12401−12402 and references therein.

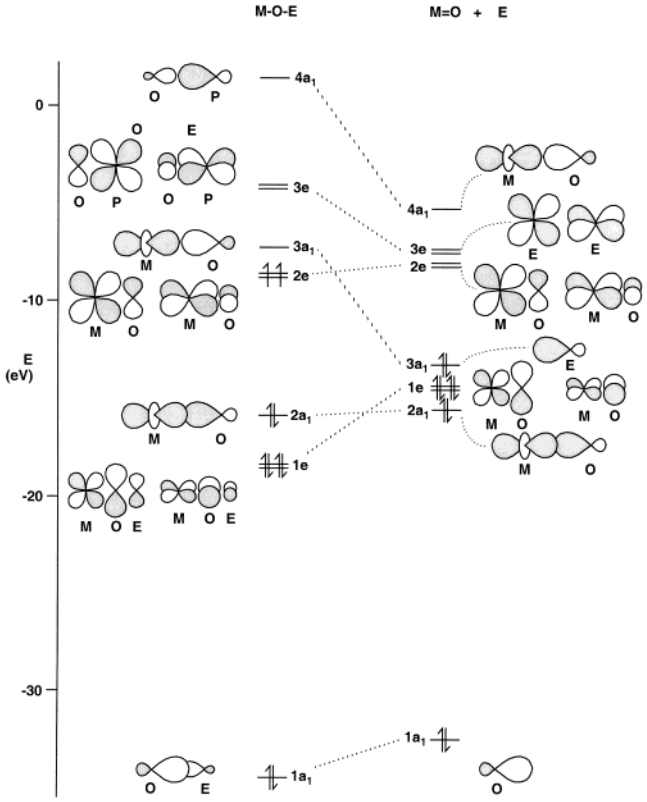

Figure 7. Orbital correlation diagram for generic L_nM-O-E (MOE) $\rightleftarrows$ L_nMO (MO) + E (E = substrate); energetics are based on EHMO calculations of $(HO)_3VOPMe_3$ (**3′**-$OPMe_3$), PMe_3, and $(HO)_3VO$ (**2′**-V). Reactant ($S = 1$) states efficiently intersystem cross with product $S = 0$ states when reactant excited states with populated σ^*-orbitals are mixed in effectively; the reduction in symmetry upon bending M−O−E facilitates this process.

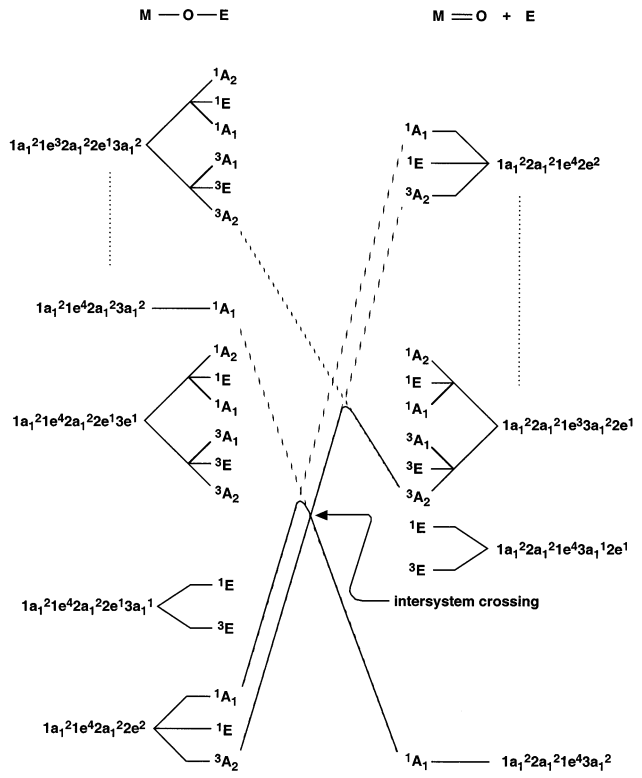

Figure 8. Truncated electronic state diagram (C_{3v}) for generic L_nM-O-E (MOE) $\rightleftarrows$ L_nMO (MO) + E (E = substrate) showing only critical state correlations (solid lines) and correlations of electronic configuration (dashed lines); energetics are based on EHMO calculations of $(HO)_3VOPMe_3$ (**3′**-$OPMe_3$), PMe_3, and $(HO)_3VO$ (**2′**-V).

R_3PO (R = Me, Ph, ^{t}Bu) Deoxygenations. 1. Relative Rates. As previously noted, phosphine oxide adducts of $(silox)_3V$ (**1**-V) are the thermodynamic sinks in that system. For niobium and tantalum, there exists a curious dichotomy between substrates R_3PO (R = Me, Ph) and $^tBu_3PO$. While the former are rapidly deoxygenated by $(silox)_3Ta$ (**1**-Ta) and $(silox)_3NbL$ (**1**-NbL, L = 4-pic, PMe_3) at 23 °C, with the subtle exception of inhibition by released 4-picoline, neither system reacts with $^tBu_3PO$, even at elevated temperatures. Since the gas-phase deoxygenation of Ph_3PO is considered to be only 6 kcal/mol easier than that of Me_3PO,[52] it does not seem likely that the electronic difference upon replacing a Me with a ^{t}Bu would render deoxygenation rapid in the former, yet nonexistent in the latter! Perhaps the widely disparate sterics of the two substrates plays a role.

2. Orbital Correlation Diagram. For a simple visualization of the O-atom transfer event, an EHMO calculation,[75] whose results are indicated in Figure 7, was done on a linear reactant $(HO)_3V-O-PMe_3$ (**3′**-$OPMe_3$ = M−O−E) and its products, oxide $(HO)_3VO$ (**2′**-V = M═O) and PMe_3 (E). The first-row metal was chosen because of the relative energies of the fragments, and the ease and accuracy of the calculation. Aside from the energies, the general features will be the same for niobium, tantalum, and a variety of substrates (E).

The adduct M−O−E features a triplet ground state with the HOMO being a degenerate set of vanadium−oxygen π-antibonding orbitals (2e) that are half-occupied. Below are only two σ-type orbitals that essentially describe the E−O ($1a_1$) and M−O ($2a_1$) single bonds, and the fully occupied π-bonding orbital 1e. The M−O−E intermediate possesses one net π- and two σ-interactions. In the products, oxygen ($1a_1$) and substrate ($3a_1$) lone pairs constitute low-lying σ-type orbitals in addition to the M−O σ bond ($2a_1$). The metal−oxygen π-bonding orbital 1e is also fully occupied. The contradiction between adduct M−O−E, and oxo M═O and E is readily apparent. In order for the reactant to generate products in a symmetry-allowed process, both must have the same number and type of orbitals. The disallowed nature of the reaction may be overcome if two electrons on the reactant side are promoted from 2e to $3a_1$, or two electrons on the product side are promoted from $3a_1$ to 2e, thereby equalizing the populated orbital types. Promotions of one electron for both reactant and products can also lead to correlation, but no matter how the process is viewed, excited states must be utilized in the transformation.

3. State Correlation Diagrams. Figure 8 illustrates the roughly energetically ordered electronic states of $(HO)_3V-O-PMe_3$ (**3′**-$OPMe_3$ = M−O−E) and $(HO)_3VO$ (**2′**-V = M═O) + PMe_3 (E) critical to understanding the O-atom

(75) Extended Hückel molecular orbital (EHMO) calculations were conducted using the HyperChem program: HyperChem(TM), Hypercube, Inc., 1115 NW 4th St., Gainesville, FL 32601.

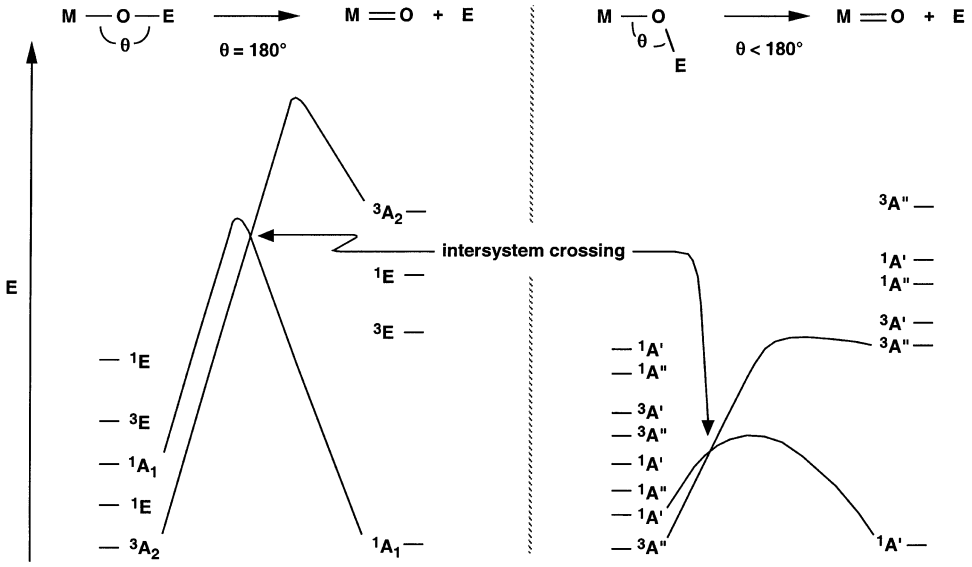

Figure 9. Truncated electronic state correlation diagram for generic L_nM-O-E (MOE) $\rightleftarrows$ L_nMO (MO) + E (E = substrate) showing how the reduction in symmetry upon bending M−O−E facilitates atom transfer by reducing the intersystem crossing barrier through mixing.

transfer reaction, including their electron configurations of origin. While the $^3A_2$ ground state of M−O−E correlates with an excited state of M=O possessing triply and singly occupied 1e and 2e orbitals, respectively, its orbital correlation is with a much higher $^3A_2$ state, hence the symmetry-allowed transformation, i.e., reactant $^3A_2 \rightarrow$ product $^3A_2$, may have a substantial energetic barrier depending on how well those product states mix. The same is true for the product $^1A_1$ ground state, which correlates with an excited state derived from the lowest electronic configuration. Its orbital correlation is with a much higher energy state, thus this transition also has a potentially large barrier that depends on how well the $^1A_1$ reactant excited states mix.

It is likely that the transformation from $(HO)_3V-O-PMe_3$ (**3′**-$OPMe_3$ = M−O−E) to $(HO)_3VO$ (**2′**-V = M=O) + PMe_3 (E) would be adiabatic, because intersystem crossing in a transition metal based system is not rigorously forbidden due to a variety of factors (e.g., spin−orbit coupling, low symmetry, etc.). As a consequence of the state correlations, the point of intersystem crossing that is necessary for conversion of the $^3A_2$ reactant to $^1A_1$ products is relatively high in energy, and deoxygenation can have a significant barrier.

Figure 9 reveals how the barrier to deoxygenation is most easily lowered. Consider the M−O−E angle (θ) to deviate from 180° (C_{3v}). The A_1 and A_2 states become A′ and A″, respectively, and various E states split into A′ and A″ states as the symmetry is lowered to C_s. The intersystem crossing point is thereby lowered for several reasons. A lower $^1A'$ state on the left now correlates with the M=O + E ground state on the right, while a lower $^3A''$ state on the right now correlates with the M−O−E ground state on the left. Greater mixing is facilitated by the splitting of E states, which are basically π-type in C_{3v}, into A′ and A″ states in C_s that permit σ-character to be introduced; correspondingly, π-character is mixed into states that were previously purely σ. Basically, as θ decreases, the orbitals lose their distinctive π- or σ-character and their admixtures allow the barriers connecting the $^1A'$ and $^3A''$ states to be energetically lowered; therefore, the intersystem crossing point is lowered as well.

4. Steric Factors and Deoxygenation. Deoxygenation of R_3PO (R = Me, Ph) by $(silox)_3Ta$ (**1**-Ta) and $(silox)_3NbL$ (**1**-NbL, L = 4-pic, PMe_3) occurs swiftly because the substrate is allowed to access the metal center via the side of the OP linkage, which is the equivalent of accessing the bent M−O−E adduct addressed above. Attack at the side of the PO bond, or at oxygen such that M−O−P is substantially less than 180°, permits P−O cleavage to occur with facility due to the consequences of lower symmetry elaborated above. If the substrate is small enough, R_3PO may also attack empty π-type orbitals on the metal.

Substrates such as $(silox)_3WNO$ (**10**) and $^tBu_3PO$ are restricted by sterics in their approach to $(silox)_3M$ (**1**-M, M = V, Nb, Ta). The nitrosyl deoxygenation is unusually slow despite a great thermodynamic impetus because the geometry for O-atom transfer is required to be nearly linear by steric factors, and the resulting intersystem crossing point remains energetically high. Similar conformational factors completely shut down the deoxygenation of $^tBu_3PO$ relative to other pathways even though there is clearly room to bind the substrate, as the structure of $(silox)_3VOP^tBu_3$ (**3**-P^tBu_3) indicates.

5. General Observations. The generality of symmetry considerations and the impact of electronic states in atom transfers bears some additional scrutiny. Woo[76] rationalized differences in reactivity of (por)Cr=O/(por)CrCl and (por)-Cr=O/(por)Cr substrates with respect to the stabilities of a $[(por)Cr-O-Cr(por)]^n$ ($n = 0, +1$) intermediate ($n = +1$) and product ($n = 0$) based on Hoffmann's relevant treatment of iron porphyrins.[77] Jahn−Teller distortions in the mixed-valence intermediate are proposed to induce degradation and

(76) Woo, L. K.; Goll, J. G.; Berreau, L. M.; Weaving, R. *J. Am. Chem. Soc.* **1992**, *114*, 7411−7415.
(77) Tatsumi, K.; Hoffmann, R. *J. Am. Chem. Soc.* **1981**, *103*, 3328−3341.

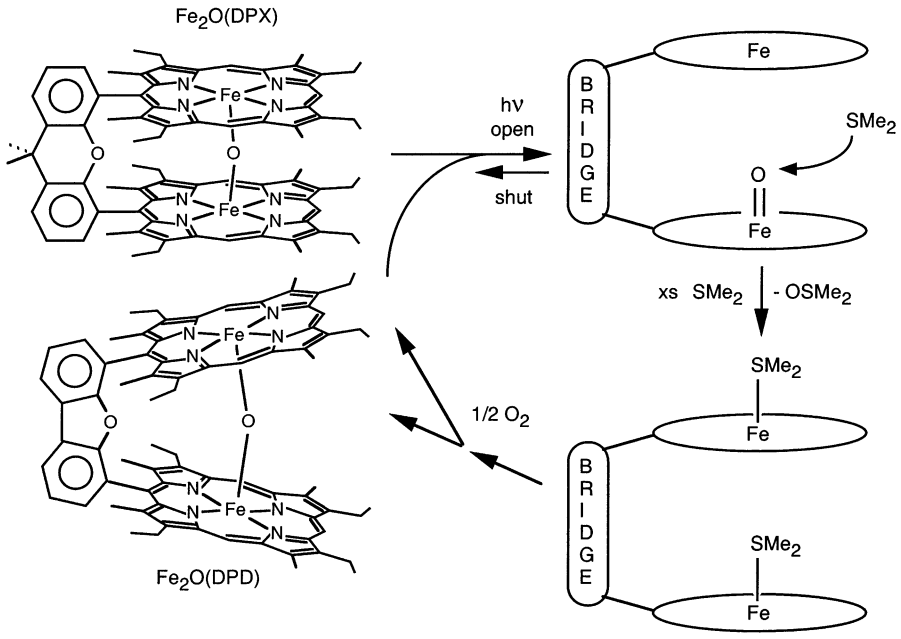

Figure 10. Cofacial bis-porphyrin O-atom transfer system developed by Nocera et al. (ref 33) illustrating likely side-on attack of the FeO by the substrate SMe_2.

oxygen/chloride self-exchange, while the Cr(III)−O−Cr(III) species was stable. While it is conceivable that electronic state changes directly impact the *kinetics* of μ-oxo formation and disruption in relation to the O-atom transfers (vide supra), this aspect of the chemistry was not discussed.

More recently, Nocera has utilized μ-O-diiron cofacial bis-porphyrins to examine O-atom transfer from ferryl groups generated upon photolysis.[33] As Figure 10 illustrates, the more flexible (DPD)Fe_2O system transferred an O atom to substrate dimethyl sulfide $\sim 10^3$ times more efficiently than the rigid (DPX)Fe_2O analogue. Two factors are likely to be at play: (1) once the ferryl is generated photochemically (photochemical activation is likely to be bridge-independent), the kinked DPD pincer has a smaller recombination rate constant than the DPX system, and (2) the more open DPD system permits swifter substrate attack than the more constrained DPX ligand. With both ligands, there is little doubt that substrate attack occurs in a side-on fashion, and the DPD system approaches that of an unbridged control.

Perhaps the most notable systems in which state selective chemistry has been proferred are those of cytochrome P450[3] and related oxomanganese O-atom transfer agents.[8,9] In the former, Shaik has developed models based on DFT calculations that suggest that cytochrome P450 is highly dependent on environment, and that different electronic states may mediate different reaction paths. In the latter, Groves attributes differing rates of oxo transfer from Mn(V)O derivatives as reflecting spin state crossover effects.

Theopold has argued that spin crossover processes are generally very swift. In a CO substitution study, no appreciable diminution of rate was observed even though diamagnetic $Tp^{iPr,Me}Co(CO)_2$ loses CO to afford paramagnetic $Tp^{iPr,Me}Co(CO)$.[78] In another investigation involving O-atom transfer from Cr(V), i.e., Cp/Cp*$CrCl_2O$ plus ethylene,[32] the spin crossing event (Cr(V) → Cr(III)) occurs after initial C−O bond formation, and it is argued that such a process is relatively inconsequential, especially since it is likely to occur with facility. While this combination of experiment and DFT calculations is compelling, the stepwise transfer of oxygen to the substrate and the nature of the intermediate Cr(IV)-$OCH_2CH_2^{\bullet}$ species possibly render this example distinct from the O-atom transfers above.

While not initially considered examples of symmetry and geometry constraints, certain reactions and observations warrant closer inspection. The enantioselective epoxidation of olefins catalyzed by (salen)XMnO derivatives is thought to occur via a Mn(V) oxo that is sterically "blocked" by 2,4-*tert*-butyl phenoxide substituents, forcing the substrate to approach over a 1,2-diiminocyclohexane backbone that relays its conformation to the prochiral face of the approaching olefin (Figure 11a).[15−17] While it seems reasonable that the *tert*-butyl groups dissuade approach of the substrate from the phenolic side of the chelate plane, the angle of approach over the cyclohexane is considerably open, as the figure ($\theta = 0-90°$) illustrates. If the symmetry and geometry factors above are also applicable in this case, the approach of the substrate olefin is constrained to be substantially away from $\theta = 0°$. The high enantioselectivities observed by Jacobsen et al. are more easily rationalized at such severe approach angles, where the influence of the cyclohexane backbone is likely to be maximized. In partial corroboration, DFT calculations on oxotransferase models manifest transition states with M−O−E angles of $\sim 130°$.[6]

In another case, Mayer et al. concluded that the lack of phosphine oxide deoxygenation by WCl_2L_4 (L = $PMePh_2$,

(78) Detrich, J. L.; Reinaud, O. M.; Rheingold, A. L.; Theopold, K. H. *J. Am. Chem. Soc.* **1995**, *117*, 11745−11748.

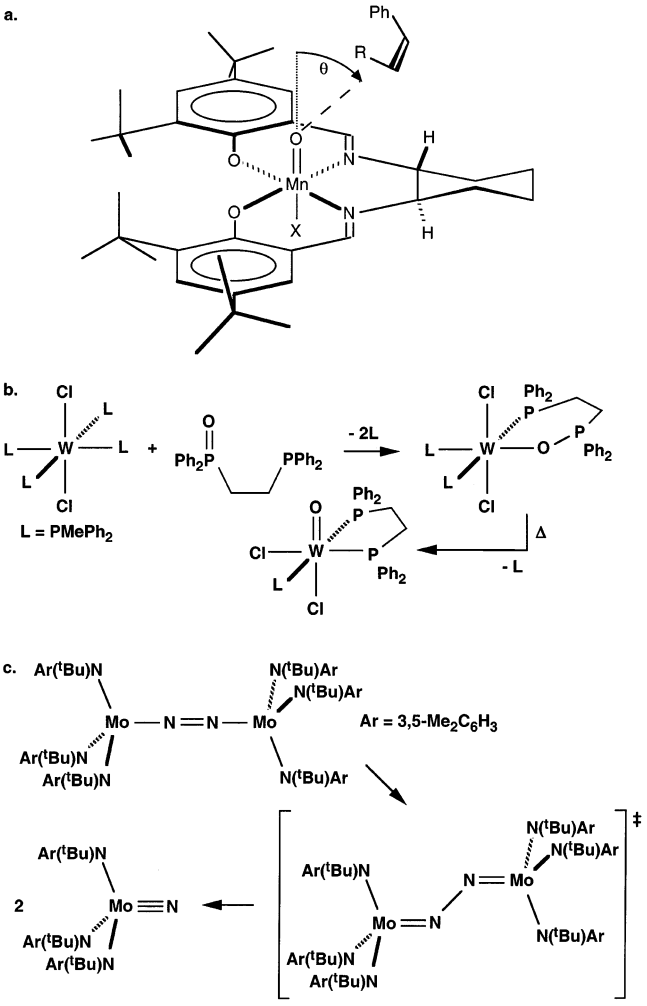

Figure 11. Possible examples of symmetry constraints on atom transfer: (a) Jacobsen's catalyst imparts enantioselectivity via high θ approach by substrate olefin; (b) chelation of phosphine/phosphite ligand of Mayer et al. (ref 79) permits orientation favorable toward OAT; (c) Cummins et al. (ref 80) show that μ-N_2 ligand splits via "kinked" transition state.

PMe_3) was due to a kinetic barrier, because rudimentary thermodynamic arguments clearly portrayed the process as favorable.[25,79] As Figure 11b shows, deoxygenation does take place if the substrate is the chelate, $Ph_2PCH_2CH_2Ph_2$-PO. The authors originally suggested that chelation was necessary to overcome the intrinsically weak binding by phosphine oxides, but isolation of the intermediate WCl_2-$\{OPPh_2CH_2CH_2Ph_2P\}(PMePh_2)_2$ revealed that additional factors contribute to the slowness of the subsequent O-atom transfer event, which is observed upon heating.[71] It is plausible that the chelate, whose W−O−P angle is probably near 120°, suffers from the same electronic factors expressed above. During thermolysis, the W−O−P angle may approach 90°, thereby allowing the symmetry constraints to be overcome by the more favorable geometry for atom transfer.

Finally, the interplay of electronic states and symmetry/geometry critical to the above chemistry is not restricted to O-atom transfers, but is generally applicable to bond-making and -breaking events that apparently transpire via linear transition states, yet actually occur via bent variants. A prominent example is recent discovery of Mo(III)-mediated dinitrogen cleavage.[80] The conversion of $2\{^t$Bu(3,5-$Me_2C_6H_3)N\}_3$Mo and N_2 to 2 equiv of nitride, $\{^t$Bu(3,5-$Me_2C_6H_3)N\}_3$MoN, has been estimated to occur with $\Delta H° \sim -86$ kcal/mol.[81] Despite the favorable thermodynamics, the enthalpic barrier from $[\{^t$Bu(3,5-$Me_2C_6H_3)N\}_3$Mo$]_2(\mu$-$N_2)$ to the nitride is large ($\Delta H^‡ = 23.3$ (3) kcal/mol), and DFT calculations suggest that a "kink" in the MoNNMo linkage is required for dinitrogen scission to take place (Figure 11c.). The linear dinitrogen complex contains three filled σ orbitals (the two MoN bonds and the NN bond), whereas the product nitrides contain four (the MoN and N lone pairs) pairs of electrons of σ-character. The "kink", or deviation of the MoNN angle from linearity, has the same effect as the bending of the M−O−E angle in O-atom transfer. The symmetry lowering permits σ/π mixing and allows triplet/singlet intersystem crossing to occur at a lower energy, rendering the cleavage allowable.

In a related case,[82] Brown noted that a nitride heterocoupling reaction to give N_2 based on the combination of Os(VI) and Mo(VI) nitrides occurred with far greater facility than the corresponding self-coupling reactions.[83] Since it is likely that the formation of N_2 from two Os(VI) nitrides is more thermodynamically favorable than the heterocoupling event, it was concluded that the asymmetry of the reaction, in this case the favorable polarization of the transition state due to the disparate metals, was playing an important role.

Even in cases where the symmetry is low enough that *formal* electronic state changes are not critical, bond scission events do not occur in a linear fashion. Parkin[84] has recently observed the thermal degradation of $Cp^*_2Mo(N_3)_2$ to Cp^*_2-$MoN(N_3)$ and has utilized DFT calculations to examine its energetics. Not only are the Mo−N−N bonds bent throughout the course of the reaction in response to electronic factors that reflect the EAN rule, but the N−N cleavage itself occurs via a bent N−N−N geometry and $\Delta H^‡$ is appreciable (26.6-(2) kcal/mol). Additional orbital considerations establish the best geometry for generation of the azide−nitride product. It is interesting that the dinitrogen cleavage of Cummins and this seemingly differrent azide cleavage apparently share a similar degradation path independent of electronic state requirements. The results support the contention that linear bond cleavage events that are not of the donor/acceptor type are intrinsically disfavored relative to bent transition states.

(79) Brock, S. L.; Mayer, J. M. *Inorg. Chem.* **1991**, *30*, 2138−2143.

(80) Laplaza, C. E.; Johnson, M. J. A.; Peters, J. C.; Odom, A. L.; Kim, E.; Cummins, C. C.; George, G. N.; Pickering, I. J. *J. Am. Chem. Soc.* **1996**, *118*, 8623−8638.

(81) Cherry, J.-P. F.; Johnson, A. R.; Baraldo, L. M.; Tsai, Y.-C.; Cummins, C. C.; Kryatov, S. V.; Rybak-Akimova, E. V.; Capps, K. B.; Hoff, C. D.; Haar, C. M.; Nolan, S. P.*J. Am. Chem. Soc.* **2001**, *123*, 7271−7286.

(82) Seymore, S. B.; Brown, S. N. *Inorg. Chem.* **2002**, *41*, 462−469.

(83) Ware, D. C.; Taube, H. *Inorg. Chem.* **1991**, *30*, 4605−4610.

(84) Shin, J. H.; Bridgewater, B. M.; Churchill, D. G.; Baik, M.-H.; Friesner, R. A.; Parkin, G. *J. Am. Chem. Soc.* **2001**, *123*, 10111−10112.

In summary, the effects of differing electronic states on atom transfers, ligand dynamics,[85] ligand substitution or loss,[34,35,86−88] CH-bond activation, and presumably a variety of other transition metal reactions, while often difficult to detect, can be profound.

Conclusions

Specific. In the systems studied, the deoxygenations of $(silox)_3WNO$ (**10**) and R_3PO (R = Me, Ph, ^{t}Bu) by $(silox)_3M$ (**1**-M, M = V, Nb, Ta), the linear transfer of an oxygen atom is forbidden by symmetry, and a significant barrier for the process is apparent, even for cases with a large thermodynamic driving force. Degradation of an intermediate $(silox)_3M-O-E$ (**1**-MOE) species via deoxygenation is facilitated by bending the M−O−E angle that enables a lowering of the barrier via the electronic consequences of lower symmetry. There is a related symmetry barrier for the docking of a substrate (EO) to $(silox)_3Ta$ (**1**-Ta) due to its singlet ground state. In order to form adducts, the triplet state of **1**-Ta must be accessed, or the EO molecule must approach the molecule such that the Ta−O−E angle deviates substantially from 180°.

A Valence Bond Viewpoint. Pedagogically, the discussions above can be simplified and generalized within a valence bond framework. In a simple treatment for a linear O-atom transfer, one is only required to count the number of filled σ-type orbitals on each side of the equation; if they are the same, then O-atom transfer is allowed. For example, where M = $(silox)_3Ta$ (**1**-Ta), formation of the adduct $(silox)_3Ta-O-E$ (e.g., E = PR_3) is forbidden because the pair of electrons in **1**-Ta reside in a σ-type orbital, d_{z^2}. In combination with the EO σ-bond and O σ-lone pair, these 6 σ electrons are two more than what resides in the σ-bonds of linear $(silox)_3Ta-O-E$. Only when the triplet state is accessed can **1**-Ta bind the substrate. Likewise for O-atom transfer from $(silox)_3M-O-E$ ($S = 1$) to $(silox)_3MO + E$, the adduct has 6 π-electrons (2 in a degenerate d_{xz}/d_{yz} set; 4 in O pπ-orbitals) and 4 σ-based electrons (the M−O and O−E bonds), but the products have only 4 π-bonding electrons (MO π-bonds) and 6 σ-type (lone pairs on O and E, and the MO σ-bond). This O-atom transfer is symmetry forbidden unless M−O−E bending allows the mixing that turns an O pπ-orbital into one of predominantly σ-character.

Experimental Section

General Considerations. All manipulations were performed using either glovebox or high vacuum line techniques. Hydrocarbon solvents containing 1−2 mL of added tetraglyme, and ethereal solvents were distilled under nitrogen from purple benzophenone ketyl and vacuum transferred from same prior to use. Benzene-d_6 was dried over activated 4 Å molecular sieves, vacuum transferred, and stored under N_2; toluene-d_8 and THF-d_8 were dried over sodium benzophenone ketyl. All glassware was oven-dried, and NMR tubes were additionally flame-dried under dynamic vacuum. Gaseous reagents (NO, N_2O (Matheson)) were used as received and passed over a −78 °C trap when possible. $\{(Me_3Si)_2N\}_3V$[36] and $(silox)_3NbCl_2$[29] were prepared via literature methods, and $(silox)_3WCl_2$ (**5**) and $(silox)_3WCl$ (**6**) were prepared according to previous work.[43]

NMR spectra were obtained using Varian XL-400, INOVA-400, and Unity-500 spectrometers, and chemical shifts are reported relative to benzene-d_6 (^{1}H, d 7.15; ^{13}C, d 128.39), THF-d_8 (^{1}H, d 3.58; ^{13}C, 67.57), toluene-d_8 (^{1}H, d 2.09; ^{13}C, 20.40), and cyclohexane-d_{12} (^{1}H, d 1.38; ^{13}C, 24.6). Infrared spectra were recorded on a Nicolet Impact 410 spectrophotometer interfaced to a Gateway PC. Magnetic measurements were conducted via the Evans method.[37] Elemental analyses were performed by Oneida Research Services, Whitesboro, NY, or Robertson Microlit Laboratories, Madison, NJ.

Procedures. 1. $(silox)_3V$ (1-V). A 100 mL flask was charged with $\{(Me_3Si)_2N\}_3V$ (1.74 g, 3.27 mmol) and hexanes (20 mL). An addition funnel, containing 2.5 equiv (use of <3.0 equiv minimized impurities) of ^{t}Bu$_3$SiOH (1.77 g, 8.18 mmol) in hexanes (20 mL), was attached. The ^{t}Bu$_3$SiOH/hexanes solution was added dropwise over 15 min and the resulting solution stirred for 1.5 h before all volatiles were removed. The resulting purple residue was triturated with pentane (2 × 10 mL), dissolved in pentane (20 mL), and filtered. The filtrate was reduced to 10 mL, cooled to −78 °C, and filtered, providing **1**-V as a purple powder (1.40 g, 74% yield based on ^{t}Bu$_3$SiOH).

2. $(silox)_3VO$ (2-V). A 25 mL flask was charged with **1**-V (300 mg, 0.43 mmol), a gas bulb was attached, and the system was evacuated. Benzene (15 mL) was condensed and nitrous oxide (88 Torr) was passed over a dry ice/acetone trap and condensed from a 108.4 mL gas bulb at 77 K. Upon thawing the purple solution quickly turned light beige and N_2 evolved. The solution was stirred for 45 min, and all volatiles were removed, leaving **2**-V as an off-white powder (220 mg, 72% yield).

3. $(silox)_3VOPMe_3$ (3-OPMe$_3$). A 10 mL flask was charged with **1**-V (150 mg, 0.215 mmol) and Me_3PO (22 mg, 0.237 mmol). The system was evacuated, and benzene (8 mL) was condensed. Upon thawing, the solution immediately turned emerald green. After stirring for 45 min all volatiles were stripped and the resulting green solid was triturated with pentane (2 × 6 mL). Pentane (3 mL) was condensed and the insoluble product filtered to obtain **3**-OPMe$_3$ as dark green microcrystals (101 mg, 60% yield).

4. $(silox)_3VOPPh_3$ (3-OPPh$_3$). A 10 mL flask was charged with **1**-V (150 mg, 0.215 mmol) and Ph_3PO (66 mg, 0.24 mmol). The system was evacuated, and benzene (6 mL) was condensed. Upon thawing, the solution immediately turned bright green. After stirring for 30 min all volatiles were stripped and the resulting green solid was triturated with pentane (3 × 5 mL). Pentane (6 mL) was condensed and the insoluble product filtered to obtain **3**-OPPh$_3$ as dark green microcrystals (166 mg, 80% yield).

5. $(silox)_3VOP^tBu_3$ (3-OP^{t}Bu$_3$). A 10 mL flask was charged with **1**-V (150 mg, 0.215 mmol) and ^{t}Bu$_3$PO (22 mg, 0.237 mmol). The system was evacuated, and benzene (8 mL) was condensed. Upon thawing, the solution immediately turned emerald green. After stirring for 45 min all volatiles were stripped and the resulting green solid was triturated with pentane (2 × 6 mL). Pentane (3 mL) was condensed and the insoluble product filtered to obtain **3**-OP^{t}Bu$_3$ as dark green microcrystals (79 mg,75% yield).

(85) Smith, K. M.; Poli, R.; Legzdins, P. *Chem. Eur. J.* **1999**, *5*, 1598−1608.
(86) Smith, K. M.; Poli, R.; Harvey, J. N. *New J. Chem.* **2000**, *24*, 77−80.
(87) Franke, O.; Wiesler, B. E.; Lehnert, N.; Näther, C.; Ksenofontov, V.; Neuhausen, J.; Tuczek, F. *Inorg. Chem.* **2002**, *41*, 3491−3499.
(88) (a) Smith, K. M.; Poli, R.; Harvey, J. N. *Chem. Eur. J.* **2001**, *7*, 1679−1690. (b) Green, J. C.; Harvey, J. N.; Poli, R. *J. Chem. Soc., Dalton Trans.* **2002**, 1861−1866.

6. (silox)$_3$NbPMe$_3$ (1-NbPMe$_3$). A 100 mL flask was charged with (silox)$_3$NbCl$_2$ (**4**, 3.0 g, 3.7 mmol) and 2.5 equiv of Na/Hg (22.5 g, 0.95% Na). The system was evacuated, and trimethylphosphine (40 mL) was condensed. Upon thawing, the solution turned light blue and then bright purple-blue after several hours with obvious salt formation. The solution was stirred overnight, and all volatiles were removed. The residue was triturated with hexanes (3 × 15 mL), dissolved in hexanes (20 mL), and filtered through Celite (1 in.) and the salt cake was washed repeatedly. The filtrate was condensed to 10 mL, cooled to −78 °C for 2 h, and filtered to provide **1**-NbPMe$_3$ as a bright purple crystalline solid (1.6 g, 53% yield).

7. (silox)$_3$ClWO (7). A solution of (silox)$_3$WCl (**6**, 520 mg, 0.601 mmol) in 12 mL of hexane was prepared, and 1.4 equiv of N_2O was admitted from a gas bulb into the flask at −196 °C. Upon warming to 25 °C, the solution changed from green to colorless and gas evolution was apparent. The solution was concentrated to 2.5 mL and cooled to −78 °C to yield 320 mg of faint pink crystals (60%). An assay by ^{1}H NMR spectroscopy indicated less than 1% (silox)$_3$WCl$_2$ (**5**). IR (Nujol, cm^{-1}): 934 (w), 920 (ν(WO), m), 858 (s), 813 (s), 722 (m), 629 (m).

8. (silox)$_3$WO (8). (silox)$_3$ClWO (**7**) (236 mg, 0.268 mmol) was placed in a flask with 1.5 equiv of 0.5 wt % Na/Hg (1.85 g, 0.402 mmol of Na). THF (10 mL) was added at −78 °C, and the mixture was allowed to slowly warm. The solution became deep purple as it reached 25 °C, and stirring was continued for another 30 min. The solvent was removed, and the residue was triturated with hexanes (3 × 5 mL), resulting in conversion of the hexane-insoluble purple solid (possibly [(silox)$_3$ClWO]Na(THF)$_x$) to a green-brown hexane-soluble material that was dissolved in pentane and filtered through Celite. The solution was concentrated to 1.5 mL, cooled to −78 °C to precipitate a gray-green solid, and filtered. The product (**8**) was collected (50 mg, 22% yield), but a ^{1}H NMR spectral assay revealed the presence of 2−3% unidentified impurities. An Evans method measurement gave μ_{eff} = 1.24 μ_B when corrected for diamagnetic impurities. IR (Nujol, cm^{-1}): 933 (w), 909 (ν(WO), m), 845 (s), 814 (s), 722 (m), 627 (m).

9. (silox)$_3$ClWNO (9, with Byproducts 5 and 10). To a flask containing 150 mg (0.173 mmol) of **6** was added 10 mL of hexane. After dissolution, the solution was frozen at −196 °C and 3 equiv of NO was admitted via a gas bulb. The flask was warmed to −78 °C, and upon thawing the solution turned deep red with some red precipitate. The mixture was stirred for an additional 5 min at −78 °C, and the excess NO was removed. The solvent was stripped under vacuum as the reaction mixture warmed slowly to 23 °C. The resulting red solid (132 mg, roughly 85% material yield, 66% yield of **9**) was observed (^{1}H NMR spectroscopic assay) to contain 78% **9**, 11% **5**, and 11% **10**. The purity could not be improved by recrystallization. IR (**9**, Nujol, cm^{-1}): 1651 (ν(NO), s), 1015 (w), 1006 (w), 957 (w), 933 (m), 918 (w), 857 (s), 835 (s), 819 (s), 805 (s), 788 (br s), 627 (m).

10. (silox)$_3$WNO (10). A 25 mL flask was charged with (silox)$_3$WCl (**6**, 445 mg, 0.514 mmol) and 2 equiv of Na/Hg (3.37 g, 0.7% Na). A gas bulb was attached and the system evacuated. THF (15 mL) was condensed and allowed to thaw to dissolve all solids. The solution was frozen, and NO (173 Torr) was condensed from a 109.4 mL gas bulb at 77 K. The solution was rapidly thawed and turned red after 9 min, and the excess NO was removed. The solution was stirred for an additional 10 min before all volatiles were removed, and the resulting orange-brown residue was triturated with hexanes (3 × 10 mL). Sometimes the crude product contained as much as 25% unreacted **6** and the above procedure was repeated. The final solid was dissolved in hexanes (10 mL) and filtered through 1 in. of Celite. The salt cake was washed repeatedly and the filtrate stripped of all volatiles. Diethyl ether (4 mL) was condensed and the solution was cooled to −78 °C for 2 h and filtered to provide **10** as a light yellow powder (104 mg, 24% yield).

11. (silox)$_3$WN (11). A bomb was charged with (silox)$_3$WCl (**6**, 420 mg, 0.49 mmol), and a gas bulb was attached. The system was evacuated and benzene (10 mL) condensed. 2-Methylaziridine (66 Torr, 0.990 mmol) was condensed from a 276.5 mL gas bulb at 77 K. Upon thawing, the solution quickly turned bright blue and then light pink. The solution was stirred for a total of 15 min, and then all volatiles were removed. The resulting pink solid was dissolved in pentane (5 mL), cooled to −78 °C for 2 h, and filtered to give **4** as a light pink solid (90 mg, 22% yield) with <5% (silox)$_3$WCl$_2$ (**5**) impurity. Analytically pure samples could be prepared by repeated recrystallizations from pentane.

12. NMR Tube Reactions (General). NMR tubes were sealed to a 14/20 adapter and flame-dried under active vacuum immediately before use. The tubes were charged with reagent and substrate solids and then evacuated. An appropriate deuterated solvent was then condensed at 77K and the tube sealed under active vacuum. If a condensable (77 K) gas was a reagent, it was added via calibrated gas bulb prior to sealing of the tube. Reactions were assayed periodically by ^{1}H NMR spectroscopy.

Physical Studies. 13. Kinetics. Deoxygenations of (silox)$_3$WNO (**10**) by (silox)$_3$M (**1**-M, M = V, NbL (L = 4-pic, PMe$_3$), Ta) were monitored in NMR tubes as described in procedure 12, as were the reactions of R$_3$PO (R = Me, Ph, ^{t}Bu) with (silox)$_3$M (**1**-M, M = V, NbL (L = 4-pic, PMe$_3$), Ta). While the reactions were roughly conducted, the reproducibility of each deoxygenation was checked, and all thermolyses were conducted in constant temperature (±1 °C) oil baths.

14. Single-Crystal X-ray Diffraction Study of (silox)$_3$VOPMe$_3$ (3-OPMe$_3$). In a drybox, a 10 mL vial was charged with a solution of **3**-OPMe$_3$ (30 mg) in toluene (0.8 mL). A crystal suitable for X-ray analysis was obtained by cooling the solution for 12 h at −30 °C. An emerald green crystal (0.4 × 0.3 × 0.2 mm) was covered in epoxy and placed on the goniometer head of a Siemens SMART CCD Area Detector system equipped with a fine-focus molybdenum X-ray tube (λ = 0.71073 Å). All non-hydrogen atoms were anisotropically refined, and hydrogen atoms were treated as idealized contributions.

15. Single-Crystal X-ray Diffraction Study of (silox)$_3$VOP^{t}Bu$_3$ (3-OP^{t}Bu$_3$). A sealed tube containing a solution of **3**-OP^{t}Bu$_3$ (50 mg) in cyclohexane (0.8 mL) was slowly cooled from 155 to 25 °C. An emerald green crystal (0.2 × 0.05 × 0.05 mm) was covered in polyisobutylene and placed on the goniometer head of a Siemens SMART CCD Area Detector system equipped with a fine-focus molybdenum X-ray tube (λ = 0.71073 Å). The initial structure solution in *P*6(3)/*mmc* gave acceptable connectivity, but the displacements, interatomic distances and an $R_1 \sim 0.20$ were problematic. Twinning possibilities exist for a simulated possible space group of *P*6$_3$/*mmc*,[89] and a successful solution involved two twin fragments related by a 60° rotation along the *c*-axis in space group *P*31*c* (SHELX command: TWIN −1 0 0 1 1 0 0 0 1). Refinement then proceeded routinely with all non-hydrogen atoms anisotropically refined. Hydrogen atoms were treated as idealized contributions.

(89) *International Tables for Crystallography*; Wilson, A. J. C., Ed.; Kluwer Academic Publishers: Boston, 1995; Vol. C, p 13, Table 1.3.4.2.

Table 7. $(HO)_3M$ (**1′**-M, M = V, Nb, Ta), $(HO)_3MO$ (**2′**-M), $(HO)_3WNO$ (**10′**), and $(HO)_3WN$ (**11′**) Singlet and Triplet Energies at Various Levels of Computation, Singlet/Triplet Free Energy Differences Where Appropriate, and Free Energies of Reaction for **1′**-M + **10′** → **2′**-M + **11′**[a]

							$\Delta G(S-T)$						ΔG_{rxn}					
	1′-V (S)	**1′**-V (T)	**1′**-Nb (S)	**1′**-Nb (T)	**1′**-Ta (S)	**1′**-Ta (T)	**1′**-V	**1′**-Nb	**1′**-Ta	**10′**	**11′**	**2′**-V	**2′**-Nb	**2′**-Ta	**1′**-V (T)	**1′**-Nb (S)	**1′**-Ta (S)
G	0.00708	0.00590	0.00625	0.00378	0.00582	0.00424				0.01551	0.01362	0.01314	0.00937	0.00854				
B3LYP	−121.16108	−121.18419	−106.64513	−106.64389	−107.62382	−107.60115	15.2	0.8	−13.2	−143.49334	−127.55399	−137.20395	−122.73164	−123.71260	−50.5	−92.3	−93.8	
HF	−119.59329	−119.64857	−105.13137	−105.15602	−106.09751	−106.10218	35.4	17.0	3.9	−141.29820	−125.66514	−135.22214	−120.88312	−121.87077	40.7	−73.7	−87.5	
MP2	−120.44784	−120.46776	−105.93351	−105.93247	−106.84219	−106.81628	13.2	0.9	−15.3	−142.51988	−126.69943	−136.48526	−121.95389	−122.85332	−120.3	−124.7	−119.1	
MP3	−120.44394	−120.47042	−105.92414	−105.92711	−106.83238	−106.81016	17.4	3.4	−12.9	−142.42323	−126.60636	−136.29987	−121.88406	−122.80096	−4.5	−89.0	−94.7	
MP4D	−120.46649	−120.48946	−105.94262	−105.94390	−106.84930	−106.82531	15.2	2.4	−14.1	−142.48367	−126.66420	−136.44284	−121.92946	−122.83518	−80.7	−104.3	−103.9	
MP4DQ	−120.45561	−120.47933	−105.93271	−105.93487	−106.84070	−106.81792	15.6	2.9	−13.3	−142.45664	−126.65129	−136.42927	−121.91402	−122.82281	−87.4	−109.6	−110.4	
PUHF	−119.59329	−119.65001	−105.13137	−105.15741	−106.09751	−106.10348	36.3	17.9	4.7	−141.29820	−125.66514	−135.22214	−120.88312	−121.87077	41.6	−73.7	−87.5	
PMP2	−120.44784	−120.46883	−105.93351	−105.93343	−106.84219	−106.81715	13.9	1.5	−14.7	−142.51988	−126.69943	−136.48526	−121.95389	−122.85332	−119.6	−124.7	−119.1	
PMP3	−120.44394	−120.47140	−105.92414	−105.92787	−106.83238	−106.81083	18.0	3.9	−12.5	−142.42323	−126.60636	−136.29987	−121.88406	−122.80096	−3.9	−89.0	−94.7	
MP4SDQ	−120.48014	−120.49858	−105.94931	−105.94906	−106.85492	−106.82981	12.3	1.4	−14.8	−142.48848	−126.67558	−136.53010	−121.94758	−122.84817	−133.8	−115.5	−112.6	
CCSD	−120.47592	−120.49824	−105.94647	−105.94585	−106.85296	−106.82758	14.7	1.2	−14.9	−142.46551	−126.65007	−136.39068	−121.91889	−122.82960	−45.0	−97.7	−100.6	
CCSD(T)	−120.50900	−120.52575	−105.97229	−105.96754	−106.87579	−106.84627	11.2	−1.4	−17.5	−142.51560	−126.68879	−136.46332	−121.95889	−122.86252	−66.1	−99.5	−99.8	
S2		2.011		2.010		2.009												
S2A		2.000		2.000		2.000												

[a] Energies are reported in atomic units, all were determined at the B3LYP/SBK(d) geometry, and free energies are in kcal/mol. Thermal and entropic contributions to the Gibbs free energy (G) were determined from B3LYP/SBK(d) optimized geometry. Abbreviations: B3LYP, Becke's three-parameter exchange functional with the Yang−Lee−Parr exchange functional; HF, Hartree−Fock; MP2 and MP3, Møller−Plesset second- and third-order perturbation theory; MP4D, Møller−Plesset fourth-order perturbation theory with double excitations; MP4DQ, Møller−Plesset fourth-order perturbation theory with double and quadruple excitations; PUHF, projected Hartree−Fock (for singlet species this is the HF energy); PMP2, projected MP2 (for singlet species this is the MP2 energy); PMP3, projected MP3 (for singlet species this is the MP3 energy); MP4SQD, MP4 with single, double, and quadruple excitations; CCSD, coupled clusters with single and double excitations; CCSD(T), CCSD with triple excitations added perturbatively; S2, the expectation value of the total spin for triplet species; S2A, for triplet species, this is the expectation value of the total spin after annihilation of higher multiplicity contaminants.

16. Single-Crystal X-ray Diffraction Study of $(silox)_3NbPMe_3$ (1-$NbPMe_3$). In a drybox, a 10 mL vial was charged with a solution of **1**-$NbPMe_3$ (30 mg), hexanes (0.5 mL), and $(Me_3Si)_2O$ (0.5 mL). Crystals suitable for X-ray analysis were obtained by slow evaporation of the solvent in a refrigerator (−30 °C) over a 1 week period. A bright blue crystal (0.4 × 0.4 × 0.4 mm) was covered in epoxy and placed on the goniometer head of a Siemens SMART CCD Area Detector system equipped with a fine-focus molybdenum X-ray tube (λ = 0.71073 Å). All non-hydrogen atoms were anisotropically refined, and hydrogen atoms were treated as idealized contributions.

17. Single-Crystal X-ray Diffraction Study of $(silox)_3ClWO$ (7). Slow evaporation of a hexane solution of **7** yielded faintly pink rectangular prismatic crystals. One crystal of dimensions 0.4 × 0.3 × 0.2 mm was selected, coated in polyisobutylene, and placed under a 173 K nitrogen stream on the goniometer head of a Siemens SMART CCD Area Detector system equipped with a fine-focus molybdenum X-ray tube (λ = 0.71073 Å). All non-hydrogen atoms were refined with anisotropic displacement parameters, and hydrogen atoms were included at calculated positions.

Computational Methods. All calculations (Table 7) reported herein employ the effective core potentials (ECPs) and valence basis sets (VBSs) of Stevens et al.[61] These ECPs were derived from Dirac−Fock relativistic atomic wave functions and include all core electrons for main group elements. For transition metals (TMs) a semi-core approximation (i.e., valence and outermost core orbitals are explicitly calculated) was utilized. Transition metal and main group VBSs were valence triple-ζ and double-ζ-plus-polarization, respectively. For hydrogens, the −31G basis set was employed. This ECP/VBS scheme, designated SBK-(d), has seen wide usage with a variety of wave function types and has been found reliable for accurate modeling of the structure, energetics, and spectroscopy of a wide variety of transition metal species.[62]

Optimizations were carried out using density functional theory (DFT) methods, although little difference was found regardless of the functional employed. Reported calculations employed the B3LYP hybrid functional[63] for geometry optimization unless stated otherwise. Energies of single point coupled cluster calculations (CCSD(T)) were determined at B3LYP/SBK(d) stationary points.[64,65] Vibrational frequencies were calculated at all B3LYP stationary points to characterize the obtained points as minima or transition states. Reported Gibbs free energies include enthalpic and entropic corrections (using vibrational frequencies calculated at the B3LYP/SBK(d) level of theory) to 298.15 K and 1 atm. All calculations were performed with the Gaussian 98 suite of programs.[66]

Acknowledgment. We thank the National Science Foundation (CHE-9528914, CHE-0212147 (P.T.W.) and CHE-9983665 (T.R.C.)) for support of this research.

Supporting Information Available: Crystallographic data in CIF format. This material is available free of charge via the Internet at http://pubs.acs.org.

IC0300114